

TABLE OF CONTENTS

Section	Page
1 BEAM NORMAL SINGLE SPIN ASYMMETRY	1
1.1 Introduction	1
1.2 Available Data Set and Conditions of Experimental Data Taking	1
1.3 Extraction of Raw Asymmetries	2
1.4 Asymmetry Correction using Linear Regression	3
1.4.1 Azimuthal Acceptance Correction	6
1.5 Corrections and Systematic Uncertainties	10
1.5.1 Regression Scheme Dependence	10
1.5.2 Regression Time Dependence	11
1.5.3 Nonlinearity	13
1.5.4 Cut Dependence	13
1.5.5 Fit Scheme Dependence	14
1.5.6 Summary of Systematic Uncertainties	14
1.6 Extraction of Physics Asymmetry	15
1.6.1 Beam Polarization	17
1.6.2 Background Corrections	17
1.6.2.1 Target Aluminum Windows	17
1.6.2.2 Beamline Scattering	19
1.6.2.3 Other Neutral Background	20
1.6.2.4 Elastic Radiative Tail	21
1.6.3 Other Corrections	23
1.6.3.1 Radiative Correction	23
1.6.3.2 Detector Bias Correction	24
1.6.3.3 Q^2 Precision	24

Section	Page
1.6.4 Beam Normal Single Spin Asymmetry	25
1.7 Comparison With Model Calculation	27
1.8 BNSSA in Nuclear Targets	28
1.9 Conclusion	28
REFERENCES	30

SECTION 1

BEAM NORMAL SINGLE SPIN ASYMMETRY

1.1 Introduction

Dedicated measurements of the beam normal single spin asymmetry in inelastic e+p, and e+N scattering near missing mass, W , ~ 1.2 GeV were performed during 18 - 20 February 2012 at Hall-C of Jefferson Lab using Q-weak apparatus. The Q-weak longitudinal measurement setup [1] was used for an inelastic transverse measurement. The electron beam polarization was changed from the nominal longitudinal setup to produce fully horizontal/ vertical polarization using the double Wien filter at the injector (section ??). The torodial magnet setting was lowered to 6700 A to focus inelastically scattered electrons onto the main Čerenkov detectors.

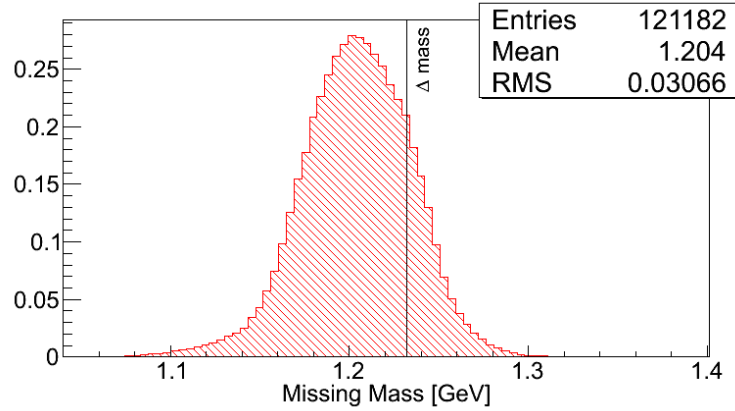


Figure 1.1 Simulated missing mass, W , distribution at the inelastic QTor setting.

1.2 Available Data Set and Conditions of Experimental Data Taking

The total collected data after hardware and software quality cuts is shown in Table 1.1. The QTor current of 6700 A selects the inelastic events near $W \sim 1.2$ GeV (Figure 1.1). Data on both sides of the inelastic peak (6000 A and 7300 A) were taken to better constrain the elastic dilution. Two transverse spin orientations, horizontal and vertical, were used. Data were collected on a liquid hydrogen (LH₂) cell, 4% thick downstream aluminum alloy (Al), and a 1.6% thick downstream carbon foil (¹²C) with 1.155 GeV beam for both spin orientations. Different beam currents were

used on different targets (see Table 1.1). The beam was rastered on the target over an area of 4 mm×4 mm by the fast raster system to minimize the target boiling or damage. The Insertable Half Wave Plate (IHWP) was used to help suppress helicity correlated beam asymmetries and was reversed at intervals of about 2 hours. More information about the conditions of data taking is given in APPENDIX-?? section ??.

Table 1.1 The transverse $N \rightarrow \Delta$ data set. The runs with vertical transverse polarization are in parentheses, the rest are from horizontal transverse polarization. Data collected in an hour was defined as run. The beam currents are shown in second to last row. Total charge on target in Coulombs is shown in the bottom row.

IHWP	QTor current					
	6000 A	6700 A			7300 A	
	LH ₂ [†]	LH ₂ [†]	Al ^{††}	¹² C	LH ₂ [†]	Al ^{††}
IN	16152	(16066)	(16067)	16150	16133	16122
	16153	16131	16115	16151	16134	16123
		16132	16116		16135	16124
						16160
OUT	16154	(16065)	(16068)			
	16156	16129	(16069)	16148	16136	16120
	16157	16130	16117	16149	16137	16121
	16158		16118			16161
			16119			
Beam current I [μ A]	180	180	60	75	180	60
Collected Data [C]	1.5	1.8 (1.9)	0.8(0.4)	0.6	2.0	0.9

In this dissertation, a full analysis of the beam normal single spin asymmetry from inelastic electron-proton scattering on LH₂ target, indicated by † in Table 1.1, will be discussed. The transverse asymmetry on Al target, indicated by †† in the table, was also analyzed as a background correction for the LH₂ target. The analysis of the remaining data are ongoing and will not be covered in this dissertation.

1.3 Extraction of Raw Asymmetries

A single detector asymmetry was obtained by averaging the two PMT asymmetries from each Čerenkov detector. The error weighted average of the asymmetries from runlets, ~ 5 minute long data samples, was extracted for a given data set. To extract the raw asymmetry A_{raw} from the detectors, the average asymmetry for the two different Insertable Half Wave Plate (IHWP) settings, IN and OUT, were determined separately for each main detector bar. The asymmetries measured in the IHWP configurations were sign corrected for the extra spin flip and averaged together after checking

for the IHWP cancellation of the false asymmetries. The error weighted value of $\langle \text{IN, -OUT} \rangle$ determined the measured raw asymmetry for each bar. These raw asymmetries were then plotted against the detector octant number, which represents the location of the detector in the azimuthal plane ($\phi = (\text{octant} - 1) \times 45^\circ$), and they were fitted using a function of the form in Equation 1.3.1. This analysis will focus on the azimuthal dependence of the detector asymmetries representing the transverse asymmetries.

$$f(\phi) = \begin{cases} \text{Horizontal transverse: } A_M^H \sin(\phi + \phi_0^H) + C^H \\ \text{Vertical transverse: } A_M^V \cos(\phi + \phi_0^V) + C^V \end{cases} \quad (1.3.1)$$

Here, ϕ is the azimuthal angle in the transverse plane to the beam direction. $\phi = 0$ indicates beam left, ϕ_0 is a possible phase offset expected to be consistent with zero. A_M is the measured asymmetry (amplitude) of the azimuthal modulation generated by BNSSA, and C is a constant appearing for monopole asymmetries such as the parity violating asymmetry generated by residual longitudinal polarization in the beam. The measured un-regressed raw asymmetries for the horizontal and vertical transverse polarization on LH₂ target are $A_{\text{raw}}^H = 5.34 \pm 0.53$ ppm and $A_{\text{raw}}^V = 4.60 \pm 0.81$ ppm respectively.

1.4 Asymmetry Correction using Linear Regression

The helicity correlated changes in the electron beam position, angle, and energy change the yield of the electrons in the detector acceptance. This can create false asymmetries in the detector and needs to be corrected before the extraction of the physics asymmetry. A multi-variable linear regression [2] is used to remove the beam asymmetries from the raw Čerenkov detector asymmetries as shown in Equation 1.4.1.

$$A_M = A_{\text{raw}} - \sum_{i=1}^6 \left(\frac{\partial A_{\text{raw}}}{\partial T_i} \right) \Delta T_i \quad (1.4.1)$$

Here A_M is the measured asymmetry after regression, and $(\partial A_{\text{raw}} / \partial T_i)$ is the detector sensitivity to a helicity-correlated beam parameter T_i with helicity-correlated differences ΔT_i . During this measurement period, the helicity-correlated differences were fairly stable except for charge (shown in Figure ??, and ??) and are summarized in Figure 1.3 and Table 1.2. The detector sensitivity slopes are calculated with linear regression, which uses natural beam motion during a runlet and considers correlations between different beam parameters. The asymmetries presented in this dissertation are

HYDROGEN-CELL (v_transverse, 6700 A): Regression-on_5+1 MD PMTavg Sensitivity. FIT = $\frac{\partial A}{\partial T} + p^T \sin/\cos$

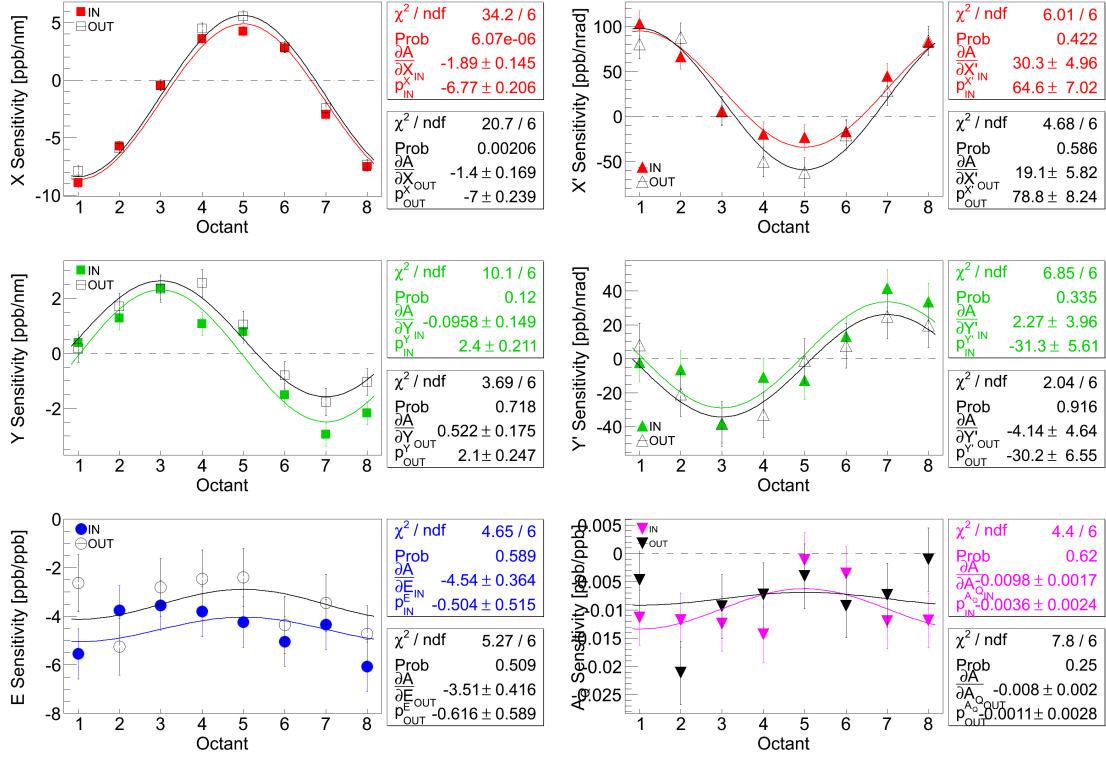


Figure 1.2 Azimuthal dependence of the main detector sensitivities to HCBA for the "5+1" regression scheme in the vertical LH₂ transverse data set are shown here. Sensitivities for beam positions and angles have sinusoidal dependence with octant. No such strong dependence is seen for energy and charge. Two IHWP states are shown separately for each beam parameter. Fit functions used to fit the parameters are shown on the plot. The constant in the fit gives the error weighted average of the sensitivities. See APPENDIX-??, section ?? for the sensitivities and corrections from full data sets.

regressed against six (5+1) beam parameters (T_i): horizontal position (X), horizontal angle (X'), vertical position (Y), vertical angle (Y'), the energy asymmetry (A_E), and the charge asymmetry (A_Q). The sensitivities of the Čerenkov detectors to different helicity correlated beam parameters have azimuthal dependence, as shown in Figure 1.2 (shown for vertical transverse data only, horizontal transverse can be found in Figure ??). This azimuthal dependence of the position and angle sensitivities are a result of the movement of the scattered electron profile across the octants which changes the effective scattering angle of the detected electrons not specific to the transverse asymmetry measurement. The position and angle sensitivities are anti-correlated. The energy and charge sensitivities are not expected to have a strong azimuthal dependence since they do not change the acceptance. The size of the applied correction to the raw asymmetries depends on the size of the

helicity-correlated beam parameter differences ΔT_i and the sensitivities $(\partial A_{\text{raw}}/\partial T_i)$. The size of the corrections were ~ 2 -3 orders of magnitude smaller than the size of the measured asymmetry and are shown in Figure 1.4 (shown for vertical transverse data only, horizontal transverse can be found in Figure ??). The total applied regression correction (Figure 1.5) is dominated by the X correction (Figure 1.4 top left). The corrections are summarized in Figure 1.6.

HYDROGEN-CELL (H+V transverse, 6700 Å): Regression-on_5+1 Beam Parameter Differences. No sign flips, or cuts applied.

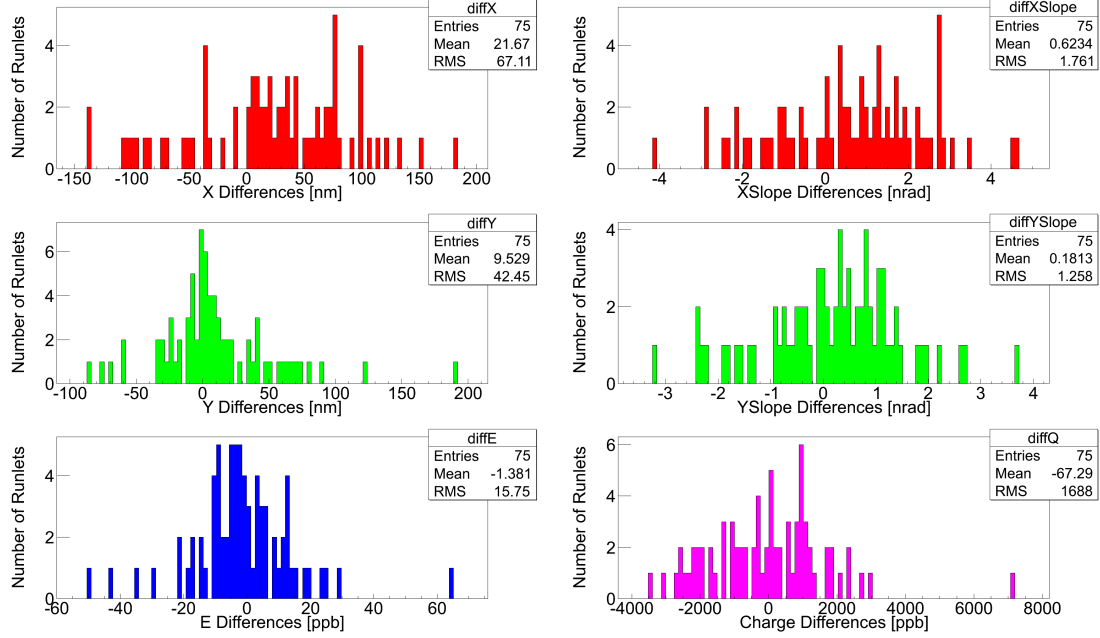


Figure 1.3 Beam parameter differences for the Hydrogen transverse data set.

The regressed “5+1” asymmetries measured using horizontal and vertical transverse polarization beam on LH₂ target are shown in Figure 1.7. The azimuthal modulating asymmetry flips sign with the insertion of the IHWP as expected. The vertical asymmetry fits may show sign of phase shift between IHWP IN and IHWP OUT settings, but may be explained due to statistical fluctuation. Transverse polarization angle was ~ 2 -3° off from ideal settings during the measurement [3,4], which can not be confirmed with the statistics in hand. The null asymmetry $(\langle \text{IN} \rangle + \langle \text{OUT} \rangle)/2$ given by the $C^{(\text{IN}+\text{OUT})/2}$ are compatible with zero within the measurement uncertainties. This indicates the azimuthal modulating signal in both IHWP IN and OUT are the same, and the non-polarization dependent false beam asymmetries were successfully removed by the regression.

The error weighted value of IN-OUT yields the measured regressed asymmetry for each bar. As expected from the azimuthal dependence of the BNSSA, there is a 90° phase offset between horizontal and vertical, as shown in Figure 1.8. The measured regressed asymmetries using hori-

Table 1.2 Beam parameter differences for the Hydrogen horizontal and vertical transverse data sets. The X differences are higher compared to Y differences.

Beam parameter differences	IHWP IN	IHWP OUT	(<IN>+<OUT>)/2	(<IN>,-<OUT>)
Horizontal Transverse				
ΔX [nm]	23.8 ± 2.1	20.6 ± 2.3	22.2 ± 1.6	3.6 ± 1.6
ΔY [nm]	6.9 ± 2.1	5.6 ± 2.3	6.2 ± 1.6	1.2 ± 1.6
$\Delta X'$ [nrad]	0.7 ± 0.1	0.7 ± 0.1	0.7 ± 0.1	0.1 ± 0.1
$\Delta Y'$ [nrad]	0.2 ± 0.1	-0.3 ± 0.1	-0.0 ± 0.1	0.3 ± 0.1
ΔE [ppb]	-2.3 ± 2.1	-1.5 ± 2.3	-1.9 ± 1.6	-0.6 ± 1.6
ΔA_Q [ppb]	8.2 ± 0.5	-237.3 ± 55.6	-114.6 ± 27.8	8.2 ± 0.5
Vertical Transverse				
ΔX [nm]	15.4 ± 3.1	58.0 ± 3.7	36.7 ± 2.4	-15.2 ± 2.4
ΔY [nm]	20.2 ± 3.1	15.4 ± 3.6	17.8 ± 2.4	5.3 ± 2.4
$\Delta X'$ [nrad]	0.6 ± 0.2	1.3 ± 0.2	1.0 ± 0.1	-0.2 ± 0.1
$\Delta Y'$ [nrad]	0.6 ± 0.2	0.9 ± 0.2	0.7 ± 0.1	-0.0 ± 0.1
ΔE [ppb]	0.5 ± 3.1	-5.4 ± 3.6	-2.4 ± 2.4	2.6 ± 2.4
ΔA_Q [ppb]	60.1 ± 0.7	158.1 ± 88.1	109.1 ± 44.1	60.1 ± 0.7

zontal and vertical transverse polarization are extracted as $A_M^H = 5.343 \pm 0.532$ ppm and $A_M^V = 4.525 \pm 0.806$ ppm respectively. The combined (error weighted average) regressed asymmetry from horizontal and vertical transverse polarization is given by

$$A_M = 5.095 \pm 0.444 \text{ ppm (stat)}. \quad (1.4.2)$$

This measurement provides a $\sim 9\%$ statistical measurement of the BNSSA in inelastic e+p scattering (not corrected for backgrounds, polarization or other experimental related systematic uncertainties). Regression has small effect on the extracted measured asymmetries ($\lesssim 4\%$).

1.4.1 Azimuthal Acceptance Correction

The acceptance of a single Q-weak Čerenkov detector is only 49% of an octant (section ??), so the reported asymmetry from a detector is an average over 22° azimuthal angle (ϕ). Each detector bar measures an average asymmetry over a range of ϕ selected by the collimators (details in [5, 6]). The effect of averaging cosines for a variable of the form $y(\phi) = A \cos(\phi + \delta)$ over the azimuthal angle yields

$$AVG[y(\phi)] = \frac{A \int_{\phi_0 - \Delta\phi}^{\phi_0 + \Delta\phi} \cos(\phi + \delta) d\phi}{(\phi_0 + \Delta\phi) - (\phi_0 - \Delta\phi)} = A \cos(\phi_0 + \delta) \times \frac{\sin \Delta\phi}{\Delta\phi}, \quad (1.4.3)$$

HYDROGEN-CELL (v_transverse, 6700 A): Regression-on_5+1 MD PMTavg Corrections. FIT = $C_T + p^T \sin/c$

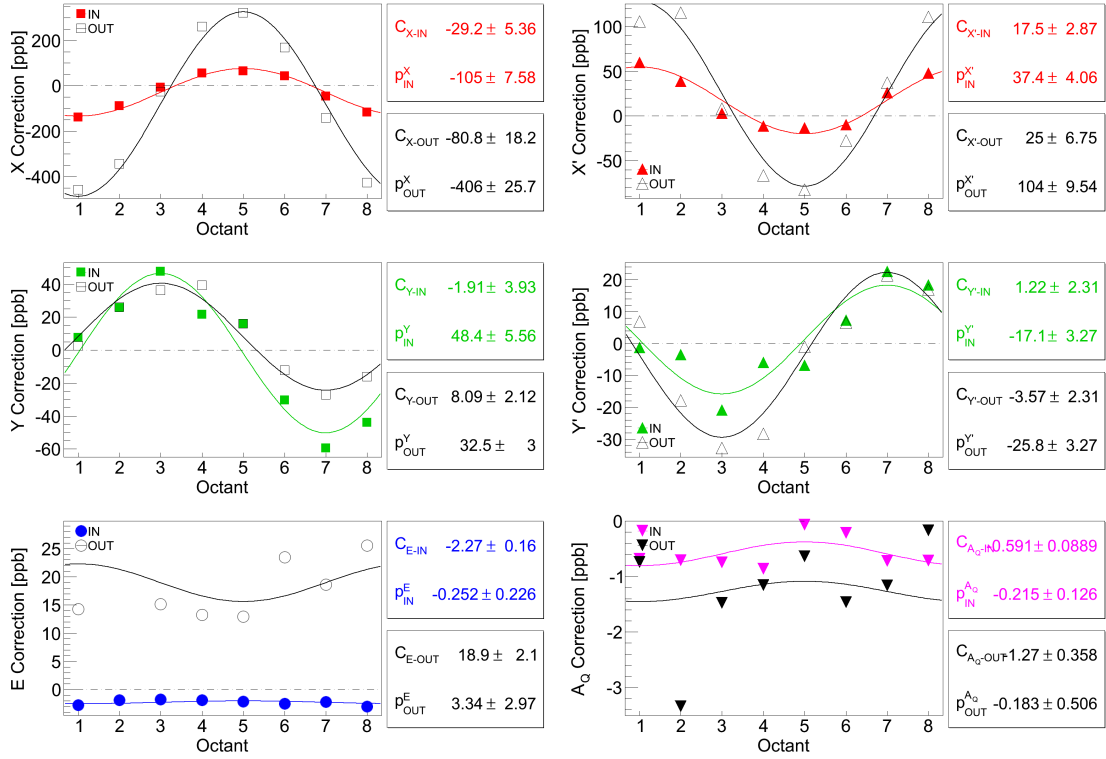


Figure 1.4 Main detector corrections (using sensitivities from “5+1” regression scheme) vs octant for vertical LH₂ transverse data set are shown here. Beam positions and angles have sinusoidal dependence with octant inherited from the sensitivities. No such dependence is seen for energy and charge. Both IHWP states are shown separately for each beam parameter.

HYDROGEN-CELL (v_transverse, 6700 A): Regression-on_5+1 MD PMTavg Corrections. FIT = $C_T + p^T \sin/c \cos(\frac{\pi}{4}(x-1))$

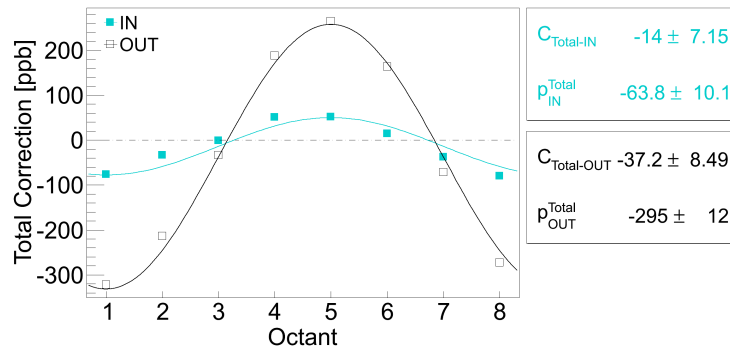


Figure 1.5 Total corrections in “5+1” regression scheme vs octant for vertical LH₂ transverse data set are shown here. The total correction is the sum of all the corrections (with sign) shown in Figure 1.4.

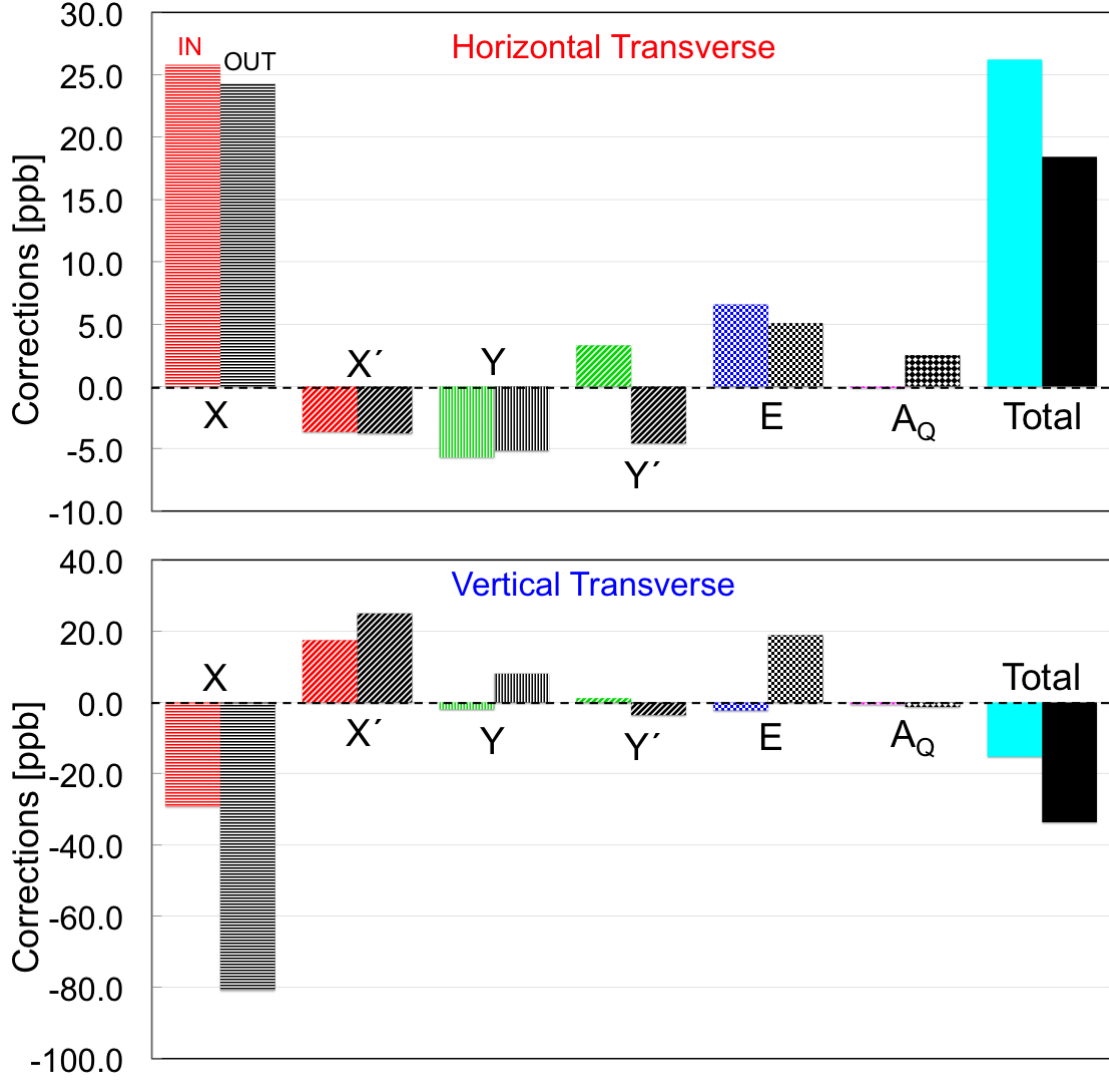


Figure 1.6 Main detector corrections (using sensitivities from “5+1” regression scheme) for horizontal (top) and vertical (bottom) LH₂ transverse data sets are shown here. Both IHWP states are shown separately for each beam parameter. The total correction is the sum of all the corrections (with sign).

where ϕ_0 is the nominal azimuthal location of the detector with $\Delta\phi$ coverage. Similarly, for sines, $AVG[y(\phi)] = A \sin(\phi_0 + \delta) \times \frac{\sin \Delta\phi}{\Delta\phi}$. So the measured asymmetry from each detector needs to be scaled by a factor of $\frac{\sin \Delta\phi}{\Delta\phi}$ to correct for the acceptance¹. $\Delta\phi = 11.025^\circ$ yields the scale factor to be $\frac{\sin \Delta\phi}{\Delta\phi} = 0.9938$. The detector acceptance corrected measured asymmetry can be extracted as

¹Here, the collimator is assumed to remove 49% of the octant acceptance (i.e 49% of 45°)

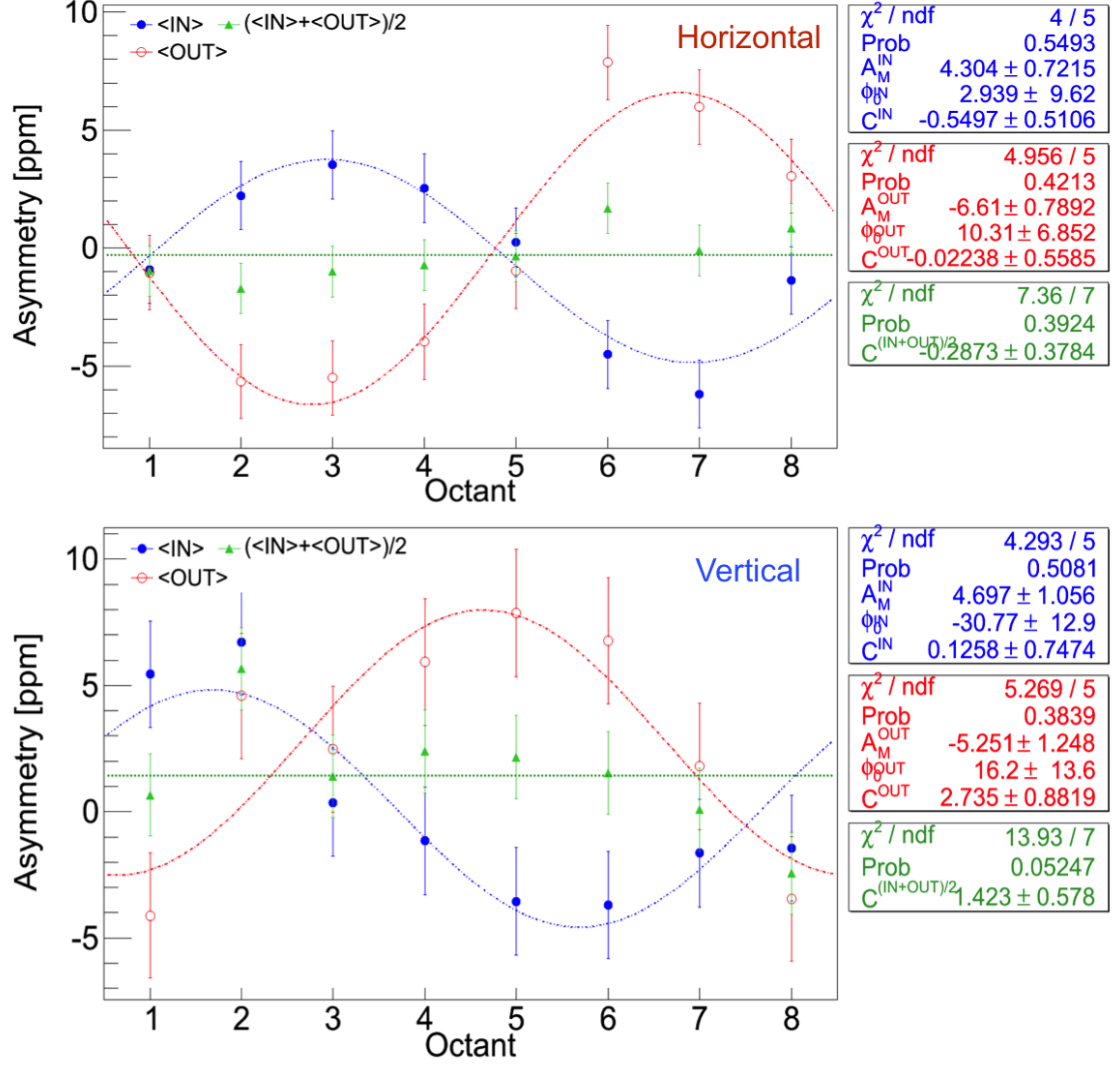


Figure 1.7 Main detector asymmetry for horizontal (top), vertical (bottom) data set. For comparison, asymmetries for IN and OUT data are also shown separately. The regressed asymmetries change sign with the insertion of the IHWP with comparable amplitudes. The $(\langle \text{IN} \rangle + \langle \text{OUT} \rangle)/2$ asymmetries of the eight Čerenkov detectors, given by $C^{(\text{IN}+\text{OUT})/2}$ is compatible with zero except in the vertical data set. The extraction of BNSSA depends on the amplitudes in the fits and by comparison of IN and OUT, not the constant term.

$$A_M^{\text{in}} = \frac{A_M}{0.9938} = 5.127 \text{ ppm.} \quad (1.4.4)$$

A conservative 50% uncertainty was used for $\Delta\phi$, which yields a systematic uncertainty of 0.004 in the correction.

HYDROGEN-CELL (transverse, 6700 A): Regression-on MD PMTavg Asymmetries. $\text{FIT}_{H/V} = A_M^{H/V} \sin/\cos(\phi) + C^{H/V}$

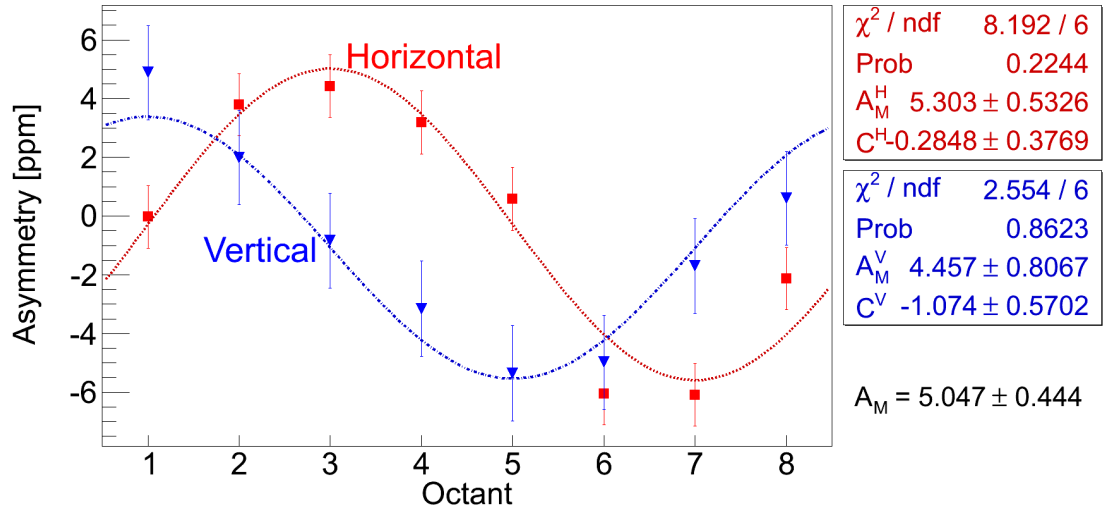


Figure 1.8 Regressed main detector asymmetry for horizontal, vertical transverse polarization are shown with red circle and blue square respectively. Data points for horizontal transverse are ~ 4 hour long measurement, whereas vertical transverse data points are ~ 2 hour long. The fit functions used are $A_M^H \sin(\phi + \phi_0^H) + C^H$ for horizontal transverse and $A_M^V \cos(\phi + \phi_0^V) + C^V$ for vertical transverse respectively. Asymmetries in each case shows $\sim 90^\circ$ phase offset, as expected between horizontal and vertical configurations.

1.5 Corrections and Systematic Uncertainties

The dominant uncertainty in the measured asymmetry for this measurement is statistical (9%). A preliminary treatment of the systematic uncertainty performed on the data set is presented in this section.

1.5.1 Regression Scheme Dependence

Since the “5+1” linear regression scheme used for this analysis is only one of the many different schemes available, it was worth investigating the scheme dependence. A list of all the independent variables for different regression sets are shown in APPENDIX-??. Ideally, the regression corrections from all the schemes should agree if all equipment is functioning properly and the regression is being done properly. Small differences in the corrections can arise from differences in the noise, resolution, and non-linear response of the monitors. To compare for the systematic studies, a common set of event cuts [7] are applied to all regression schemes to match the quartets used by each scheme. The results are summarized in Table 1.3. The regression scheme dependence uncertainty is defined as the

Table 1.3 Asymmetries from different regression schemes, along with the raw asymmetry, are shown for horizontal and vertical transverse data sets from Run 2 Pass 5 database. Corrections are small ($\lesssim 4\%$) compared to the amplitude of the measured asymmetry. The schemes without and with charge as regression variable are shown separately. Set 5 and 6 were not available due to failure of BPM 9b during Run 2. Set 9 was ignored for this analysis as it used the upstream luminosity monitor as an independent variable (more details about regression variables are in APPENDIX-??).

Regression scheme	Horizontal		Vertical	
	Asymmetry [ppm]	Correction [ppm]	Asymmetry [ppm]	Correction [ppm]
UnReg	5.339	0.000	4.602	0.000
std	5.343	0.004	4.524	-0.078
set7	5.347	0.007	4.529	-0.073
set11	5.343	0.004	4.524	-0.078
5+1	5.343	0.004	4.525	-0.077
set3	5.343	0.004	4.525	-0.077
set4	5.343	0.004	4.527	-0.076
set8	5.346	0.007	4.531	-0.072
set9	5.343	0.003	4.534	-0.069
set10	5.343	0.003	4.526	-0.077
Max - Min	set8 - set10	0.004	set8 - set11	0.006

largest difference between all of the schemes and estimated to be 0.004 ppm for horizontal transverse and 0.006 ppm for vertical transverse data set.

1.5.2 Regression Time Dependence

The standard regression algorithm works with 5 minute runlet averaged quantities. The detector sensitivities are averaged over each runlet and corresponding differences are used to correct for the false asymmetry for each quartet in the runlet. There is another systematic uncertainty associated with regression time period that is considered. The effect of using slug, few hours (~ 2), as time period for the regression instead of runlets was determined. The MD error weighted average sensitivities for a slug were calculated and average beam parameter differences for that slug were used to get the corrections, as shown in Equation 1.5.2. These slug averaged corrections were then used to regress asymmetries (Equation 1.5.1).

$$\langle A_{\text{reg}} \rangle_{\text{slug}} = \langle A_{\text{UnReg}} \rangle_{\text{slug}} - \langle C \rangle_{\text{slug}} \quad (1.5.1)$$

$$\langle C \rangle_{\text{slug}} = \sum_{i=1}^6 \left\langle \frac{\partial A}{\partial T_i} \right\rangle_{\text{slug}} \langle \Delta T_i \rangle_{\text{slug}} \quad (1.5.2)$$

where T_i 's are X , X' , Y , X' , A_E , and A_Q . The slug averaged sensitivities and beam parameter differences for the data set are shown in Figure 1.2 (also Figure ?? for horizontal transverse) and Table 1.2 respectively. The impact on regressed asymmetries due to change in the regression averaging time period for horizontal and vertical transverse data set are 0.006 ppm and 0.008 ppm respectively and are assigned as regression time dependence systematic uncertainties. More details in APPENDIX-?? section ??.

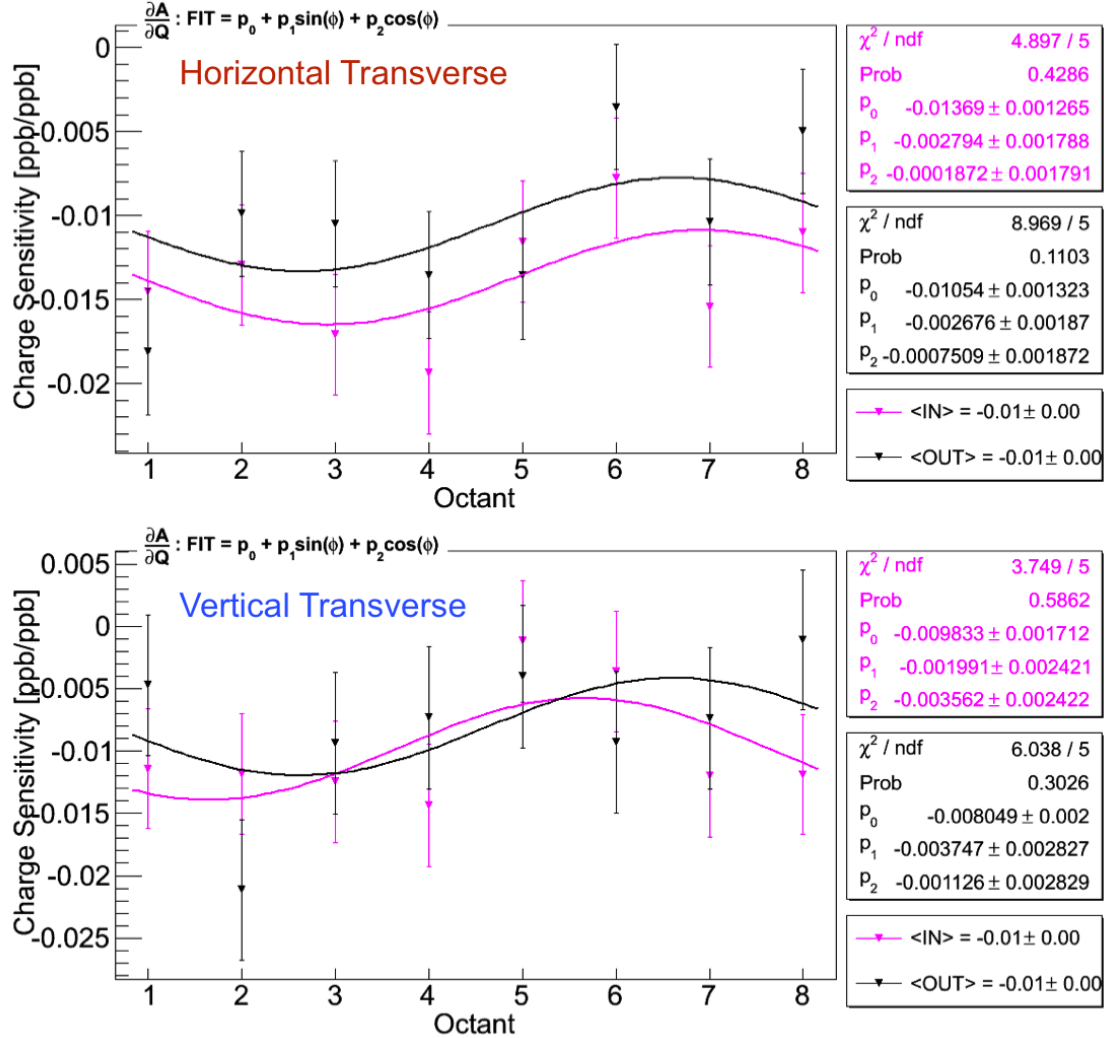


Figure 1.9 Charge sensitivity for horizontal (top) and vertical (bottom) transverse polarization data set. Average charge sensitivities of the measured detector asymmetries extracted from the six parameter (five parameter + charge) regression at beam current 180 μA . Purple (Black) represents the charge sensitivity of the IHWP IN (OUT) data which are consistent with each other. The sensitivities of the eight Čerenkov detectors vary from -0.5% to -2.0% and are stable within the running period. Average non linearity is -1% for both the cases.

1.5.3 Nonlinearity

The Čerenkov detector signals are normalized to the charge and the charge asymmetry is actively suppressed using a charge feedback system. The nonlinearity of the BCM electronics, the main detector electronics, and target density changes can induce nonlinear distortions in the charge asymmetry and hence in the measured asymmetry [8]. This nonlinearity of the system is seen to be non-zero from the non-zero charge sensitivity constant term in the (5+1) regressed detector asymmetries, as shown in Figure 1.9. For both horizontal and vertical polarization data sets, the nonlinearity is found to be -1%. At present, no proper method of handling the measured asymmetry distortion due to nonlinearity is available. The nonlinearity term is multiplied with the measured asymmetry to calculate the false asymmetry [9]. The systematic uncertainties due to nonlinearity for horizontal and vertical transverse measurements are given by 0.053 ppm and 0.045 ppm respectively.

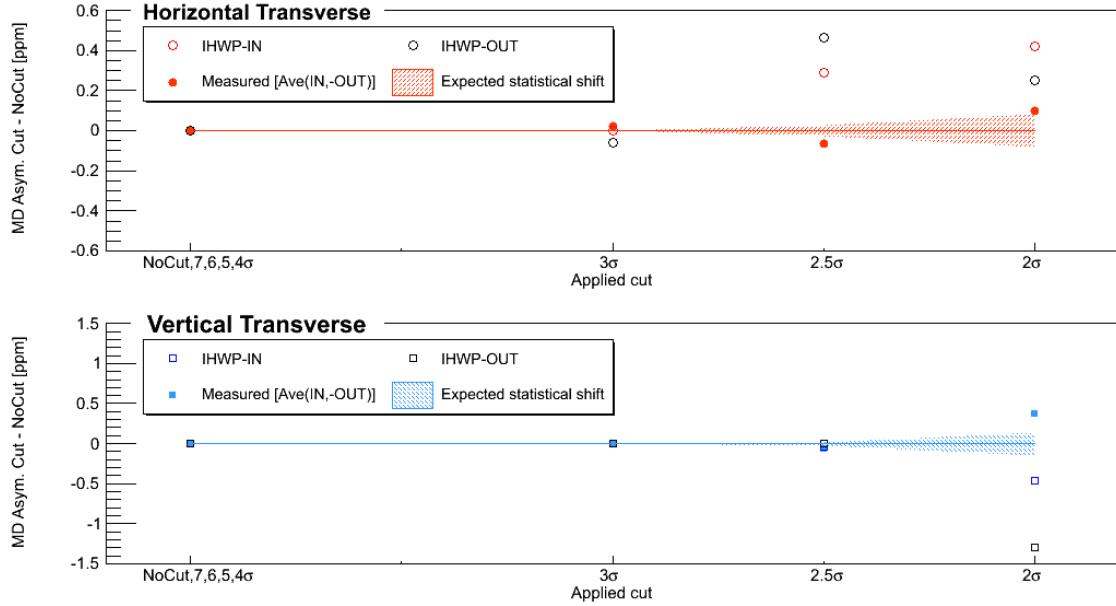


Figure 1.10 Cut dependence study. Shift in the central value of the regressed asymmetry for different cut widths for LH₂. The expected statistical shift is shown by the shaded region using the total number of quartets lost when a cut is applied to all parameters.

1.5.4 Cut Dependence

The goal of the cut dependence analysis was to assign a systematic uncertainty that comes from shifts in the mean value of the regressed asymmetry beyond statistical fluctuations after applied cuts. If linear regression is working properly, large false asymmetries in runlets with large HCBAs should be removed from the measured asymmetry after linear regression is applied and there should

not be any shift in the mean value of the regressed asymmetry beyond statistical shifts (as shown in Figure 1.10). The point-to-point uncertainty in going from cut i to cut j is estimated to be

$$\Delta_{i \rightarrow j}^{\text{pt-to-pt}} = \left(\frac{\sigma_j}{\sqrt{N_j}} - \frac{\sigma_i}{\sqrt{N_i}} \right) \quad (1.5.3)$$

Here the σ is the root mean square (RMS) of each HCBA. Inclusive cuts of 7, 6, 5, 4, 3, 2.5 and 2 σ are applied to all HCBAs and difference between regressed asymmetry with cut and without cuts are shown in Figure 1.10. The observed shift in the measured asymmetry from these cuts are larger than the expected statistical shift and 2.5 σ cuts on the HCBAs were used to assign a systematic uncertainty. The total percentage of quartets lost for cuts with respect to no cut are used to estimate the expected statistical shift, shown as the shaded region in Figure 1.10. Beyond a cut of 2.5 σ , most of the data were removed to extract a meaningful asymmetry. This analysis was performed to assign systematic uncertainty only, no data was removed from main data set. Cut dependence for horizontal and vertical transverse data set are found to be ~ 0.064 ppm and ~ 0.068 ppm respectively.

1.5.5 Fit Scheme Dependence

A sinusoidal fit to main detector octant asymmetries is used to extract measured transverse asymmetry. So it was important to find the impact of the function on fitted asymmetry. The measured asymmetry was fitted using four different functions, and the solutions are summarized in Table 1.4. The difference in measured asymmetry obtained using standard function $A_M \sin(\phi + \phi_0) + C$ and rest gives an idea about the fit function dependence of the measured asymmetry. More insightfully, the constant term in the fit function can be thought of as the apparent parity violating asymmetry contamination to the parity conserving transverse asymmetry. The size of $P_T B_n$ is much larger than $P_L A_{\text{PV}}$ so the latter has significant effect on the transverse measurement. So this PV asymmetry is buried under the fit scheme dependence and give rise to the systematic uncertainties of 0.040 ppm for horizontal and 0.083 ppm for vertical transverse data sets.

1.5.6 Summary of Systematic Uncertainties

Summary of systematic uncertainties of the measured inelastic beam normal single spin asymmetry is given in Table 1.5. The systematic studies contain uncertainties related to the extraction of the measured asymmetry such as regression, nonlinearity, cut dependence, and detector acceptance correction. The systematic studies for horizontal and vertical transverse polarization data set were performed separately; these are summarized in Figure 1.11. The statistical uncertainty weighted

Table 1.4 Fit scheme dependence of the measured asymmetry. The fit function was varied to observe the effect on measured regressed asymmetry. The difference in asymmetry between case 1 and rest are shown. Biggest offset comes from the possible phase shift.

	Fit Function	Asymmetry [ppm]	Difference (1-i) [ppm]
Horizontal Transverse			
1	$A_M^H \sin(\phi + \phi_0^H) + C^H$	5.343 ± 0.532	0.000
2	$A_M^H \sin(\phi + \phi_0^H)$	5.344 ± 0.532	0.001
3	$A_M^H \sin(\phi) + C^H$	5.303 ± 0.533	0.040
4	$A_M^H \sin(\phi)$	5.304 ± 0.533	0.039
Vertical Transverse			
1	$A_M^V \cos(\phi + \phi_0^V) + C^V$	4.525 ± 0.806	0.000
2	$A_M^V \cos(\phi + \phi_0^V)$	4.510 ± 0.806	0.015
3	$A_M^V \cos(\phi) + C^V$	4.458 ± 0.807	0.067
4	$A_M^V \cos(\phi)$	4.442 ± 0.807	0.083

average of the systematic uncertainties from horizontal and vertical transverse data sets is used for the total systematic uncertainty. The total uncertainty is the quadrature sum of the statistical and systematic uncertainties. The total uncertainty is dominated by 9% statistical uncertainty compared to 1% systematic uncertainty.

Table 1.5 Summary of uncertainties on measured asymmetry for combined horizontal and vertical data sets. The relative uncertainties are also shown in the table.

Uncertainty from	Contribution to A_M [ppm]	Relative Contribution [%]
Statistics	0.444	8.7
Regression scheme	0.005	0.1
Regression time binning	0.007	0.1
Non-linearity	0.051	1.0
Cuts	0.065	1.3
Fit scheme	0.052	1.0
Detector acceptance correction	0.016	0.3
Systematic only	0.100	2.0
Total	0.455	8.9

1.6 Extraction of Physics Asymmetry

The beam normal single spin asymmetry from inelastic e+p scattering is obtained from measured asymmetry using Equation 1.6.1 by accounting for EM radiative corrections, kinematics normalization, polarization, and backgrounds.

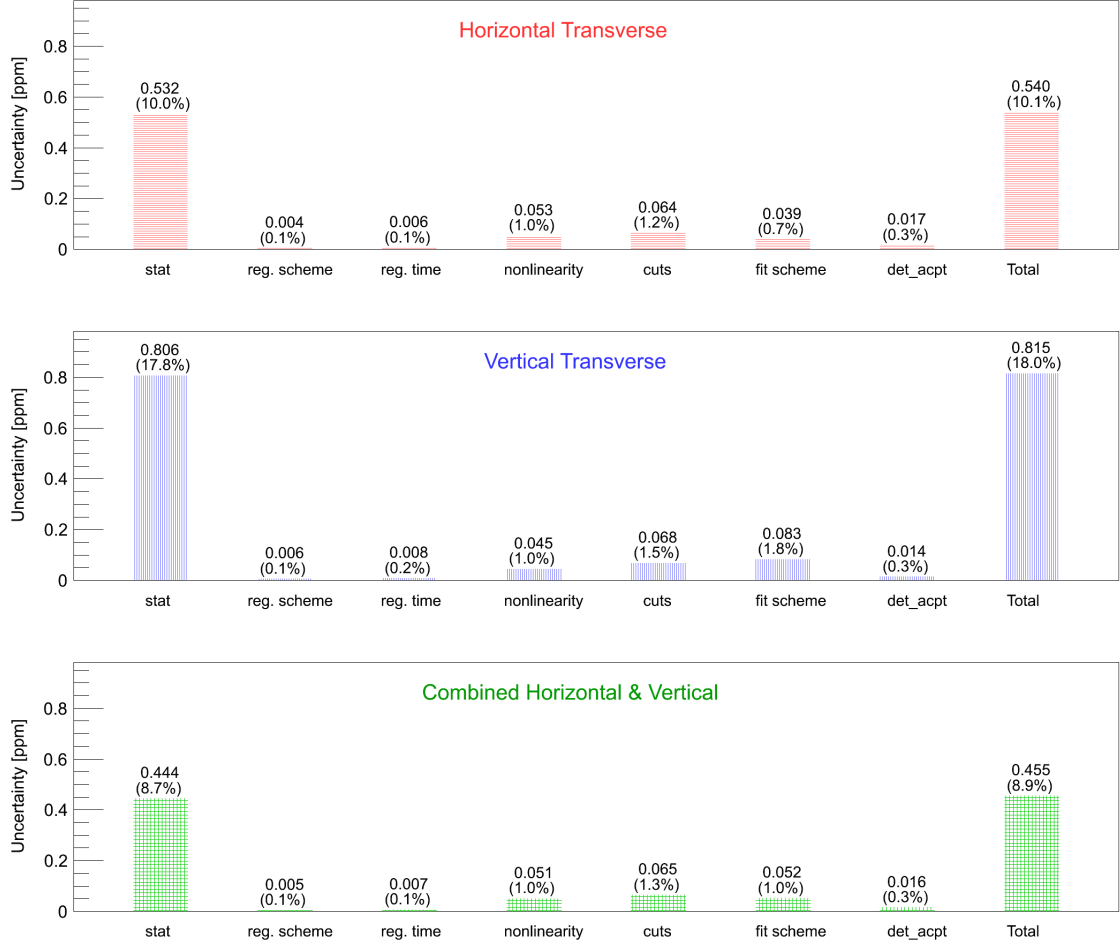


Figure 1.11 Summary of uncertainties on measured asymmetry for horizontal and vertical data set. The relative total uncertainty is dominated by statistical uncertainty compared to systematic uncertainties.

$$B_n = R_{total} \left[\frac{\left(\frac{A_M^{in}}{P} \right) - \sum_{i=1}^4 A_{bi} f_{bi}}{1 - \sum_{i=1}^4 f_{bi}} \right] \quad (1.6.1)$$

Here R_{total} is a correction factor for the experimental bias and radiative effects, P is the beam polarization, and A_{bi} is i^{th} background asymmetry with fraction of backgrounds in the total detector acceptance (dilution) f_{bi} . The corrections to the physics asymmetry and the associated uncertainties are discussed in the following sections.

1.6.1 Beam Polarization

The Hall-C Møller polarimeter and the Compton polarimeter were used to measure the beam polarization for the experiment. The photocathode Quantum Efficiency was stable and hence the beam polarization was stable for the period [10]. The Møller polarimeter is only sensitive to longitudinally polarized beam, so measurements performed with the longitudinally polarized beam right after the transverse data taking was used to determine the beam polarization. The Møller runs used for this analysis are 1593 - 1599, carried out on 20th February 2012. Each run is ~ 10 min long. Slug averaged polarizations from this Møller measurement are shown in Table 1.6. The measured beam polarization is $P = 87.50 \pm 0.28$ (stat) ± 0.74 (sys)% [11]. Details of systematic studies for the Møller polarization measurement can be found in the Q-weak internal technical document [12].

Table 1.6 Beam polarization using Møller polarimeter for Run 2 transverse data set [12].

IHWP	Polarization [%]	Statistical Uncertainty [%]
Out	87.029	0.398
In	- 87.939	0.387
Total	87.497	0.277

1.6.2 Background Corrections

The largest background source in beam normal single spin asymmetry arises from the elastic radiative tail. Small background contributions also come from electrons scattering from aluminum target windows, beamline scattering, and other soft neutral scattering. The analysis of the background asymmetries and their contributions to the BNSSA is described in the following sections.

1.6.2.1 Target Aluminum Windows

One of the important background contributions to the measured asymmetry comes from electrons scattering from the aluminum alloy target windows. Data were taken on the 4% downstream aluminum alloy target to determine the asymmetry and dilution. The measured regressed asymmetry for horizontal and vertical transverse are $A_M^{H-DSA} = 7.892 \pm 1.186$ ppm and $A_M^{V-DSA} = 9.631 \pm 1.768$ ppm [13], as shown in Figure 1.12. Combined (error weighted) regressed aluminum alloy asymmetry is $A_M^{DSA} = 8.432 \pm 0.985$ ppm. This asymmetry is then scaled by a 0.9938 for azimuthal acceptance averaging (already discussed in section 1.4.1), which yields the asymmetry as 8.484 ± 0.985 ppm. The acceptance difference between the upstream and downstream target

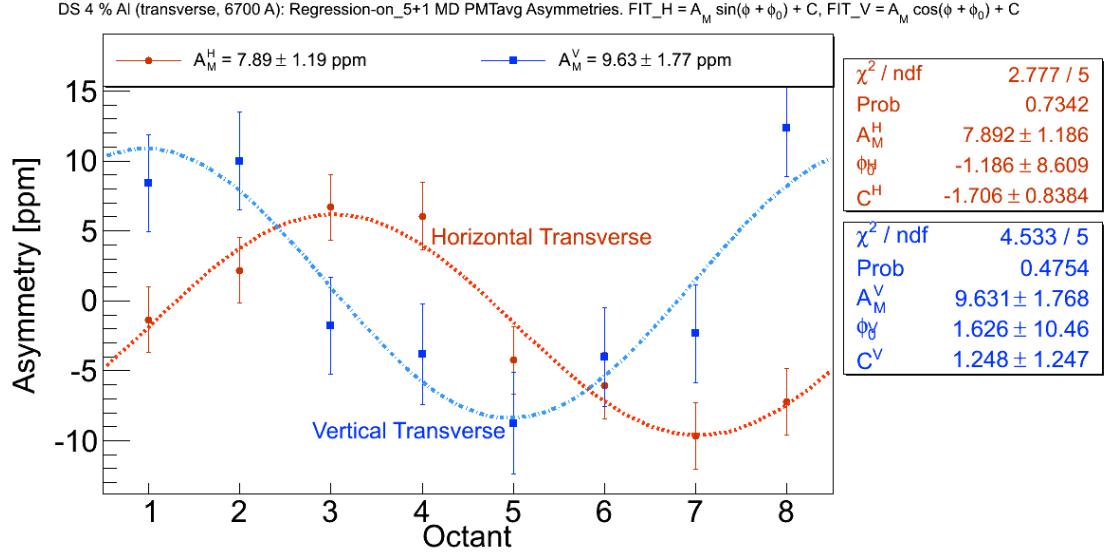


Figure 1.12 Azimuthal dependence of asymmetry from the 4% downstream aluminum target. The uncertainties are statistical only. The octant dependence in either polarization orientation are similar to what was observed for the LH₂-cell. The asymmetry is larger than the LH₂-cell asymmetry. The fit functions used for horizontal and vertical transverse data points are $A_M^H \sin(\phi + \phi_0^H) + C^H$ and $A_M^V \cos(\phi + \phi_0^V) + C^V$ respectively.

windows need to correct before the background correction. This acceptance difference causes a 20% relative difference between the mean Q^2 of the electrons coming from the upstream window compared to the downstream window, as shown in GEANT4 simulations [14] ($Q_{USAl}^2 = 0.8 \times Q_{DSAl}^2$). The beam normal single spin asymmetry from nuclei at forward angle scattering asymmetry is proportional to $\sqrt{Q^2}$ as described in theoretical models [15, 16]. So, asymmetry for upstream aluminum target can be calculated as $A_M^{USAl} = \sqrt{0.8} A_M^{DSAl} = 7.589$ ppm. Downstream and upstream aluminum target windows are expected to contribute equally [14] to the aluminum dilution in the main detector asymmetries resulting in an effective aluminum asymmetry of $A_M^{Al} = (A_M^{DSAl} + A_M^{USAl})/2 = 8.036$ ppm. An additional systematic uncertainty of $0.08 \times A_M^{Al}$ is assigned for the system non-linearity (more details in APPENDIX ??). The polarization corrected asymmetry for background windows correction is $A_{b1} = A_M^{Al}/P = 9.185 \pm 1.409$ ppm.

The measured aluminum windows dilution is $f_{b1} = 0.033 \pm 0.002$ [17]. Dedicated measurements were performed with different pressures of hydrogen gas in the target cell. Using the known pressure of hydrogen gas at different points, the pressure was extrapolated to zero.

The correction to the physics asymmetry from aluminum alloy windows is $c_{b1} = \kappa P A_{b1} f_{b1} = 1.427$ ppm, where $\kappa = (R_{total}/P)/(1 - f_{total})$.

Table 1.7 Measured asymmetry on aluminum target.

Target	Asymmetry [ppm]
DSAl	8.432
USAl	7.589
<DS+US>	8.036

USLumi Asymmetries from Longitudinal Running

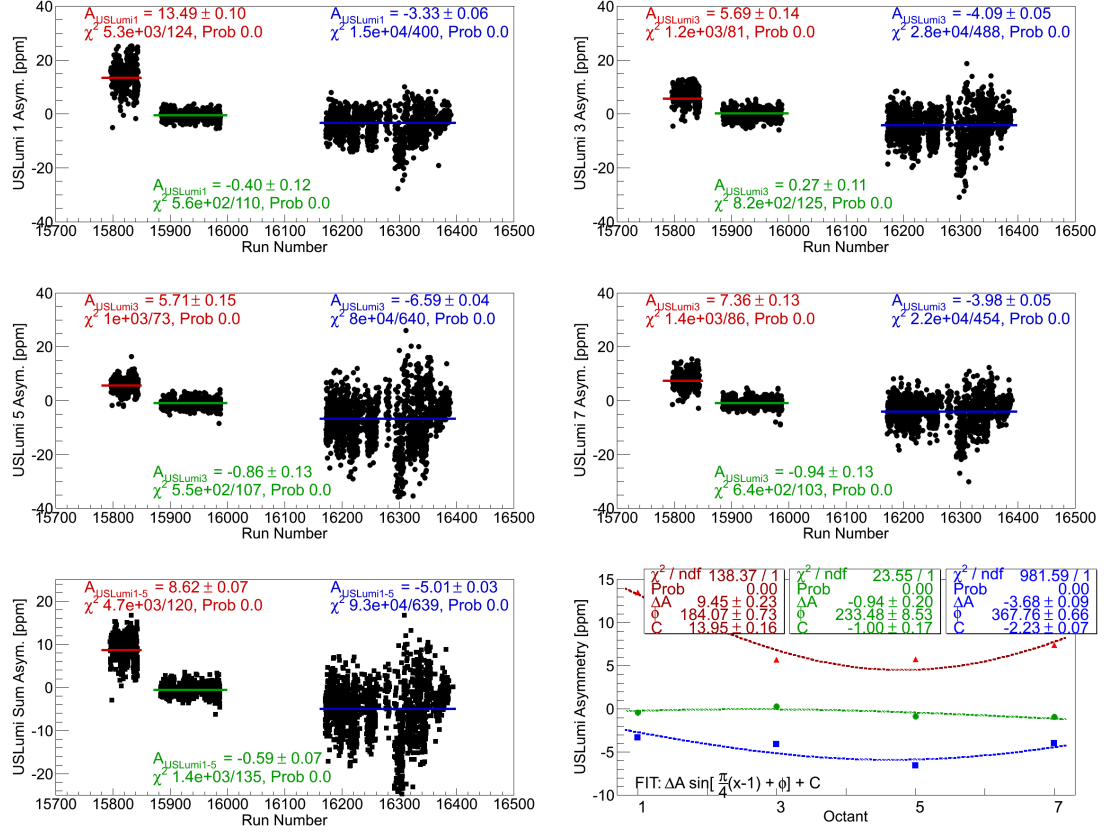


Figure 1.13 Regressed (5+1) USLumi asymmetries longitudinal running for octant 1, 3, 5, and 7 are shown in panel 1-4. USLumi sum asymmetry is shown in panel 5. Each point is a runlet. The average asymmetries vs octant for each time period are shown in panel 6.

1.6.2.2 Beamline Scattering

Another correction accounts for scattering sources in the beam line (b_2). The asymmetry (A_{b2}) was measured, along with its dilution (f_{b2}), by blocking two of the eight openings in the first of the three Pb collimators with tungsten. The measured asymmetry in the blocked octants detectors was correlated with different background detectors located outside the acceptance of the main detectors

for scaling during the primary measurement, assuming a constant dilution [18]. The variation of upstream luminosity monitor asymmetry with octant during longitudinal running can provide a good indication of the beamline scattering asymmetry. The maximum variation before and after the transverse data collection period (during longitudinal running) $\Delta A_{\text{USLumi}} = 3.534 \pm 0.16$ ppm (Figure 1.13) was used to estimate the beamline scattering asymmetry. A very simple postulate was considered: that measured main detector asymmetry has a background with a fixed fraction and an asymmetry that scales linearly with that measured in the background monitors and USLumis. The scale factor was measured directly, correlating the MD asymmetry to background asymmetries, and was estimated to be 0.0085 ± 0.0016 [19] from longitudinal period. The signal drops by an order of magnitude lower for inelastic scattering compared to elastic, whereas beamline background remains similar. Hence an additional factor of 10 was multiplied to incorporate the signal drop. The beamline background does not depend on polarization and is not corrected for it. Then, asymmetry for beam line scattering is given by $A_{b2} = \Delta A_{\text{USLumi}} \times 0.085 = 0.300 \pm 0.058$ ppm.

The beamline scattering dilution factor for inelastic running is an order of magnitude larger than in the elastic kinematic setting. The total rate at the inelastic peak drops to 10% of the total rate at the elastic peak, whereas the number of events originating in the beamline remains similar. The measured dilution for inelastic beamline scattering is 0.018 ± 0.001 [20, 21]. A 50% uncertainty on the dilution was assigned to allow the sinusoidal modulation specific to the BNSSA. The beamline scattering dilution used for the background correction is $f_{b2} = 0.018 \pm 0.009$. The correction to the physics asymmetry due to beam line scattering is $c_{b2} = \kappa P A_{b2} f_{b2} = 0.025$ ppm.

1.6.2.3 Other Neutral Background

An additional correction was applied to include soft neutral backgrounds ($b3$) arising from secondary interactions of scattered electrons in the scattered electron transport line, and was not accounted in the blocked octant studies [22]. This can arise from Møller scattering, e+p elastic scattering, etc. Simulations are in progress [23]. The other neutral background asymmetry could be as large as 5 ppm (size of the transverse asymmetry). To make the sign of the asymmetry uncertain, the asymmetry for other neutral background was assumed to be $A_{b3} = 0.000 \pm 10.000$ ppm. Here, uncertainty of 100% of the measured transverse asymmetry was assigned to give an upper bound on the neutral background asymmetry.

The neutral background dilution for the inelastic scattering has been measured as $f_{\text{neutral}} = 0.0520 \pm 0.0040$ (stat) ± 0.0014 (sys) [24]. The dilution for the other neutral background was obtained by subtracting the blocked octant background from the total neutral background measured

by the main detector and is given by $f_{b3} = f_{\text{neutral}} - f_{b2} = 0.034 \pm 0.010$. The correction to the physics asymmetry due to other neutral background is $c_{b3} = \kappa P A_{b3} f_{b3} = 0.000$ ppm.

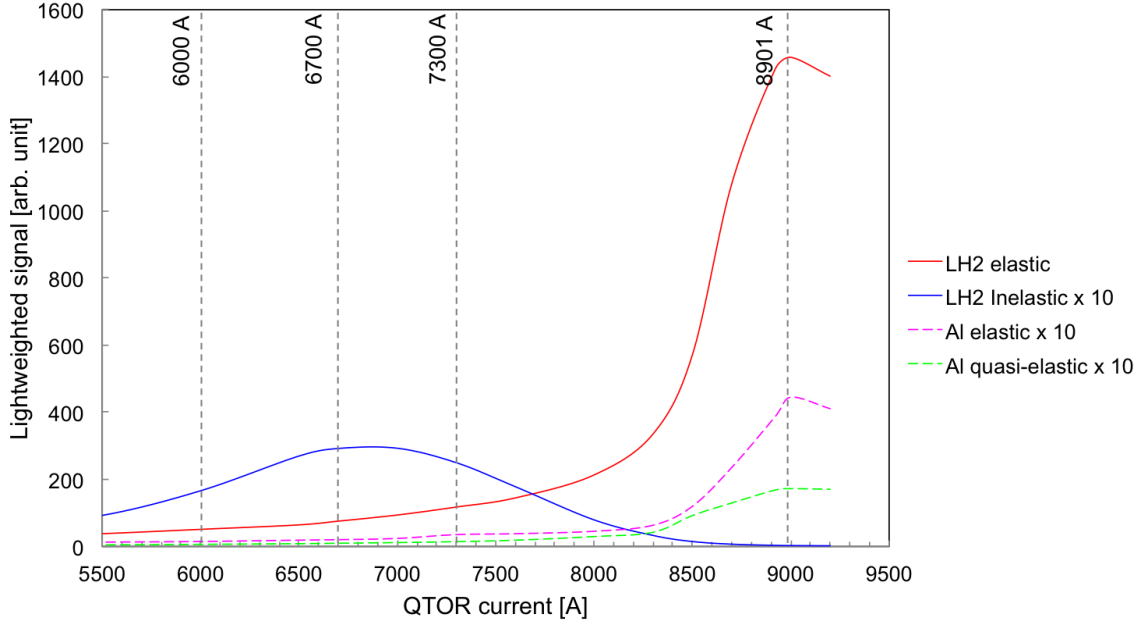


Figure 1.14 Simulation of contributions from elastic and inelastic e+p, and elastic e+Al scattering from upstream (US) and downstream (DS) target windows [25]. All but elastic e+p events have been multiplied by 10 for better visualization.

1.6.2.4 Elastic Radiative Tail

The largest background correction comes from the elastic radiative tail ($b4$). The polarization corrected measured elastic transverse asymmetry was $A_T^{el} = -5.345 \pm 0.067$ (stat) ± 0.076 (sys) ppm [26]. The elastic physics asymmetry from the LH₂-cell is similar in magnitude to the inelastic asymmetry but has the opposite sign. The elastic asymmetry was measured at $Q_{el}^2 = 0.0250 \pm 0.0006$ (GeV/c)² [27] where as inelastic measurement was at $Q_{in}^2 = 0.0209 \pm 0.0005$ (GeV/c)² (shown in Figure 1.17), hence it is necessary to scale it to the inelastic peak. The transverse asymmetry is proportional to $\sqrt{Q^2}$ [15, 16]. The polarization and $\sqrt{Q^2}$ corrected elastic asymmetry is given by $A_{b4} = \sqrt{\frac{Q_{in}^2}{Q_{el}^2}} A_T^{el} = -4.885 \pm 0.093$ ppm.

As $\sim 70\%$ of the total signal in the inelastic peak was from elastic radiative tail (Figure 1.14), it was important to tackle it carefully. A GEANT simulation was used to extract elastic dilution. Dedicated measurements were taken at both sides of the inelastic peak (at QTor current 6000 A and 7300 A) to check the simulation. A $\sim 10\%$ discrepancy was observed between current mode data and GEANT simulated signal at the inelastic peak, as shown in Figure 1.15. In order to

incorporate this discrepancy, a 10% systematic uncertainty was assigned to the elastic dilution for this preliminary analysis. A more detailed simulation is ongoing to explore this difference. The signal size for inelastic transverse is ~ 2 -3 times smaller than that of the elastic signal. Although the signal reduces for inelastic, the nonlinearity in the detector remains the same and might be responsible for this discrepancy. The simulated elastic dilution factor is given by $f_{b4} = 0.701 \pm 0.070$ [25,28]. The correction to the physics asymmetry due to the elastic radiative tail is $c_{b4} = \kappa P A_{b4} f_{b4} = -16.129$ ppm.

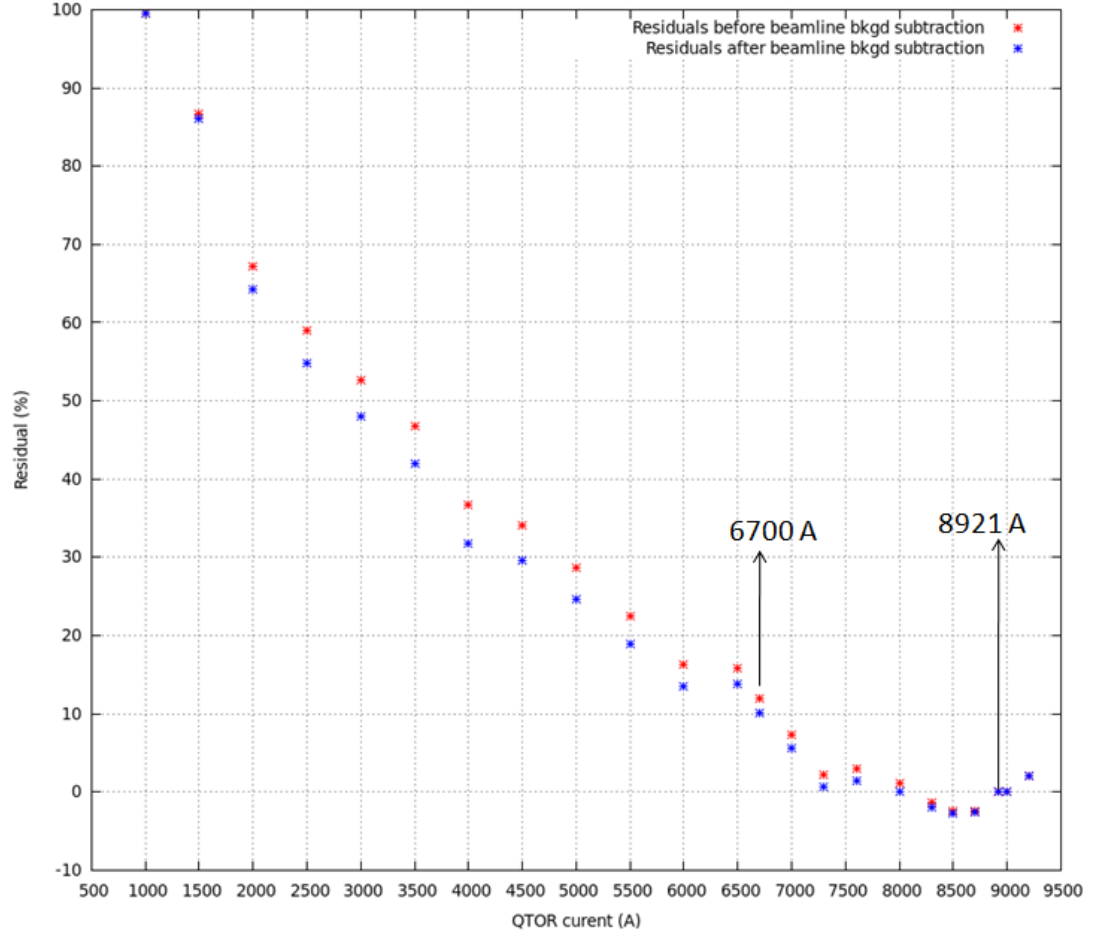


Figure 1.15 The residual of yield using Data and simulation from GEANT 3 [25] are shown in the figure. A $\sim 10\%$ discrepancy was observed at inelastic peak (6700 A) between data and simulation for matching them at elastic peak (8921 A). Beamline background correction to the yield did not improve the discrepancy.

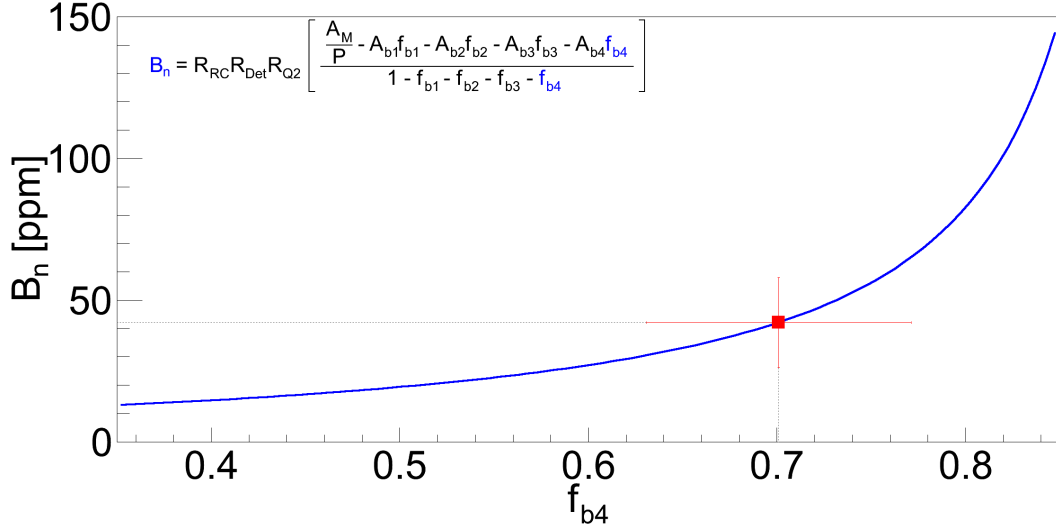
(HYDROGEN-CELL,6700A) Transverse N-to- Δ Physics Asymmetry vs Elastic Dilution

Figure 1.16 The variation of beam normal single spin asymmetry with elastic dilution.

1.6.3 Other Corrections

Another set of corrections is used to remove all the experimental bias from the measured asymmetry before extracting BNSSA. The measured asymmetry is corrected for the electromagnetic (EM) radiative corrections, light weighting on the Čerenkov detector, and Q^2 precision. These corrections are considered as independent factors and are applied to the measured asymmetry.

1.6.3.1 Radiative Correction

The energy loss and depolarization of the electrons is a result of electromagnetic (EM) radiation [29]. The measured asymmetry needs to be corrected for these EM radiative effects to obtain the beam normal single spin asymmetry at the effective Q^2 and beam polarization. The deduced radiative correction for elastic e+p scattering from simulations with and without bremsstrahlung, using methods described in Refs. [30, 31], was found to be $R_{RC} = 1.010 \pm 0.010$ [5]. The same radiative correction was used for this data set as there were no existing simulations available for inelastic e+p scattering. This correction does not have a significant impact in the final asymmetry, hence it was not unreasonable to use the existing elastic simulation result.

1.6.3.2 Detector Bias Correction

The correction between light yield and Q^2 across the detector bars affects the measured asymmetry and needs to be accounted for in the final BNSSA extraction. The multiplicative correction factor to be applied to the data is

$$R_{Det} = \frac{A_{no-bias}^{sim}}{A_{bias}^{sim}} = \sqrt{\frac{(Q^2)_{no-bias}^{sim}}{(Q^2)_{bias}^{sim}}}. \quad (1.6.2)$$

Here, A_{bias}^{sim} and $A_{no-bias}^{sim}$ are the simulated asymmetries with and without light-collection bias respectively. The detector bias correction used for this analysis is $R_{Det} = 0.998 \pm 0.002$ and is obtained using transverse simulation results [5, 32].

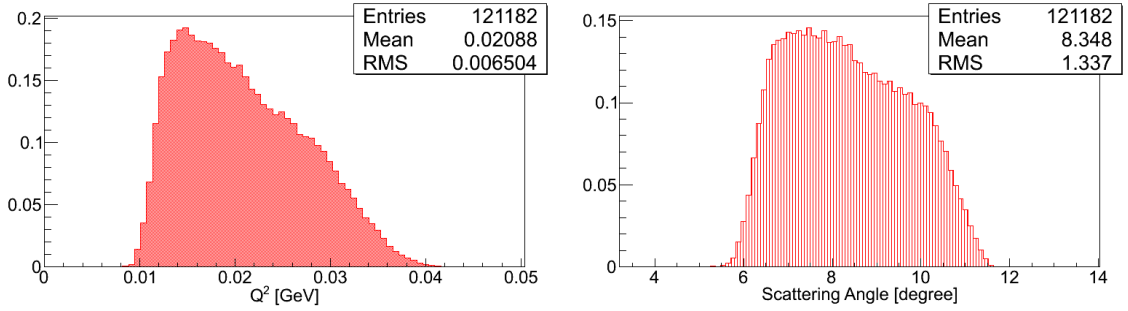


Figure 1.17 The Q^2 from GEANT 3 simulation [33]. The Q^2 was weighted by cross section and did not include any internal bremsstrahlung in the simulation (left panel). The simulated scattering angle is also shown in the right panel.

1.6.3.3 Q^2 Precision

The Q^2 for inelastic $e+p$ scattering was determined using GEANT 3 simulation and was found to be 0.0209 ± 0.0005 (GeV/c)² [33], as shown in Figure 1.17. Internal bremsstrahlung was not included in the simulation. The simulation was benchmarked by the tracking mode experimental data to represent the geometry of the experimental setup, collimation, and magnetic spectrometer. The cross section weighted Q^2 was simulated at main detector using the reaction $e + p \rightarrow e + n + \pi^+$ [33]. The two-body scattering process, and energy and momentum conservation were used to do the calculation. The scattered electron energy, and Q^2 are expressed as

$$\begin{aligned} E' &= RANDOM() \times (E_{in} - M_e) + M_e \\ Q^2 &= 4EE' \sin^2 \theta, \end{aligned} \quad (1.6.3)$$

where E_{in} is the incident beam, M_e is electron mass, and θ is scattering angle. It was important to propagate the precision of Q^2 in the final physics asymmetry. Based on theory [34], the transverse beam spin asymmetries A_N at low Q^2 behave like

$$B_n \approx \sqrt{Q^2} = m\sqrt{Q^2}. \quad (1.6.4)$$

$$dB_n = \pm \frac{1}{2} \frac{m}{\sqrt{Q^2}} dQ^2 = \pm \frac{1}{2} \frac{34.7}{\sqrt{0.02078}} 0.0005 = 0.0601 \text{ ppm} \quad (1.6.5)$$

Using Equation 1.6.4 on Q^2 and a 5 ppm measured asymmetry, the proportionality constant in the above relation can be calculated as 34.7 ppm/(GeV/c). The estimated uncertainty on the measured asymmetry due to the uncertainty in determining Q^2 is 0.061 ppm (Equation 1.6.5). A correction of $R_{Q^2} = 1.000 \pm 0.012$ was applied to include the precision in calibrating the central value of Q^2 .

1.6.4 Beam Normal Single Spin Asymmetry

Summary of required quantities to extract the beam normal single spin asymmetry from the transverse data set presented so far using

$$B_n = R_{RC} R_{Det} R_{Q^2} R_\phi \left[\frac{\left(\frac{\epsilon_{reg}}{P} \right) - A_{Al} f_{Al} - A_{QTor} f_{QTor} - A_{el} f_{el}}{1 - f_{Al} - f_{BB} - f_{QTor} - f_{el}} \right] \quad (1.6.6)$$

is shown in Table 1.8. Equation 1.6.1 has been expanded to obtain Equation 1.6.6. Using all the input values in Equation 1.6.6 gives the beam normal single spin asymmetry in inelastic e+p scattering

$$B_n = 42.27 \pm 2.45 \text{ (stat)} \pm 15.73 \text{ (sys) ppm} \quad (1.6.7)$$

for the effective kinematics of acceptance averaged electron energy $\langle E \rangle = 1.155 \pm 0.003$ GeV, $\langle Q^2 \rangle = 0.0209 \pm 0.0005$ (GeV/c)² and an average scattering angle $\langle \theta \rangle = 8.3^\circ$. The contributions from the different uncertainty sources into the final measurement are summarized in Figure 1.18. The dominant correction to the asymmetry comes from the elastic dilution tail whereas the dominant uncertainty on the measured asymmetry comes from statistics.

Table 1.8 Summary of input quantities to extract the BNSSA. The measured regressed asymmetry is corrected for detector acceptance using the factor provided in the table. The table shows the contributions of normalization factors on A_M^{in} , then the properly normalized contributions from other sources. Background corrections listed here include only $R_{total}f_i A_i/(1 - f_{total})$. Uncertainties in BNSSA due to dilution fraction and background asymmetry uncertainties are noted separately.

Input parameters			
Measured asymmetry (A_M^{in})	5.095 ± 0.455 ppm		
Beam polarization (P)	0.875 ± 0.008		
Detector acceptance correction	0.9938		
Background corrections			
Quantity	Asymmetry (A_{bi}) [ppm]	Dilution (f_{bi})	Correction $c_i = \kappa P A_{bi} f_{bi}$ [ppm]
Target windows (b1)	9.185 ± 1.409	0.033 ± 0.002	1.427
Beamline scattering (b2)	0.300 ± 0.058	0.018 ± 0.009	0.025
Other neutral bkg. (b3)	0.000 ± 10.000	0.034 ± 0.010	0.000
Elastic asymmetry (b4)	-4.885 ± 0.093	0.701 ± 0.070	-16.129
Other corrections			
Radiative correction (R_{RC})	1.010 ± 0.004		
Detector bias (R_{Det})	0.998 ± 0.001		
Q^2 acceptance (R_{Q^2})	1.000 ± 0.012		

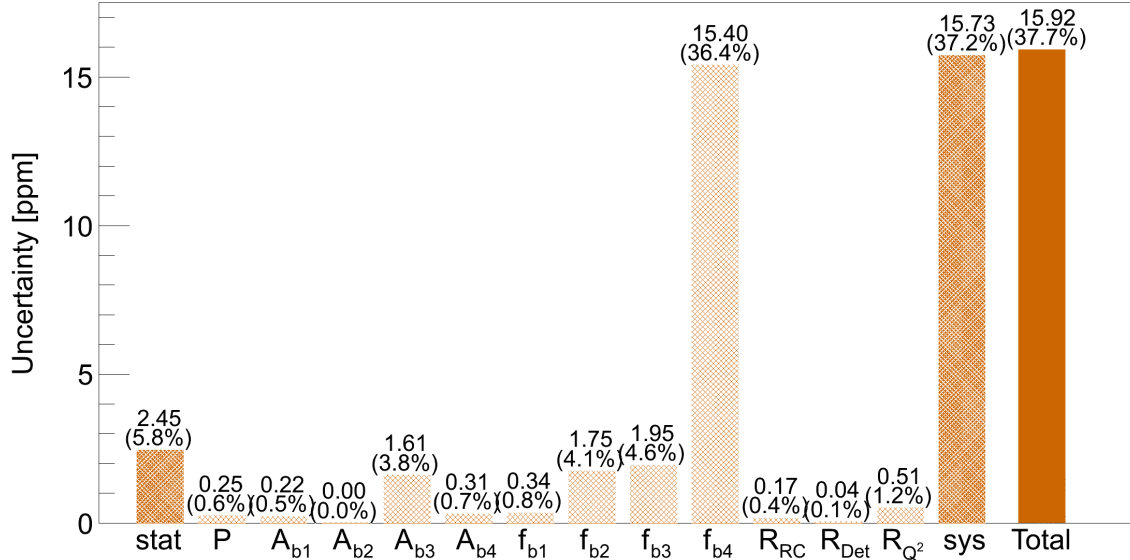


Figure 1.18 Summary of uncertainties in inelastic beam normal single spin asymmetry extraction. Measurement systematic contains the systematic uncertainties related to the extraction of the physics asymmetry such as regression, nonlinearity and acceptance averaging. The uncertainties are in ppm and the corresponding relative uncertainties are shown in parentheses.

1.7 Comparison With Model Calculation

No existing model calculation for beam normal single spin asymmetry was available at Q-weak kinematics during this analysis. Pasquini et al. [35] presented beam asymmetry in inelastic electron scattering (as shown in Figure ??) for large scattering angle at energies $E = 0.424, 0.570, 0.855$ GeV. The BNSSA were calculated separately for Δ and N intermediate states. The total asymmetry was the sum of these two intermediate states. Relatively large asymmetries were observed in the forward region; these are dominated by quasi Virtual Compton Scattering (VCS) kinematics where one exchanged photon becomes quasi-real. These asymmetries are sensitive to $\gamma^* \Delta\Delta$ form factors and can be a unique tool to study it [36].

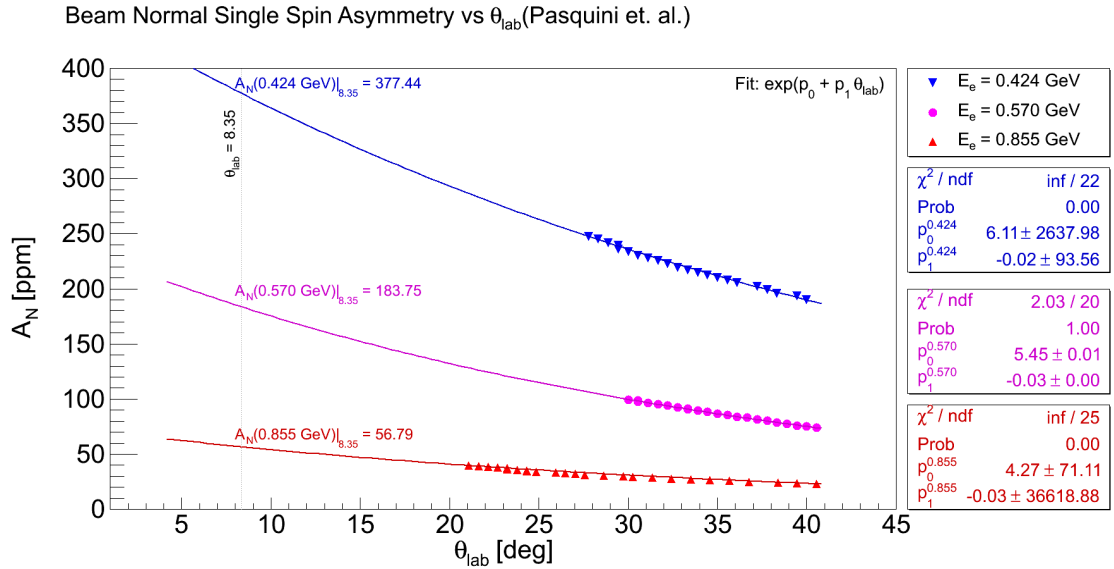


Figure 1.19 BNSSA asymmetry calculation from Pasquini et al. The points are taken from [35]. Then, the calculation is fitted with a function of the form $f(\theta_{\text{lab}}) = \exp(p_0 + p_1 \theta_{\text{lab}})$ and interpolated to Q-weak θ_{lab} value.

These asymmetries were extrapolated to forward angle down to $\theta_{\text{lab}} < 5^\circ$ using a suitable fit for all available three energies from [35], as shown in Figure 1.19. The asymmetries were obtained at $\theta_{\text{lab}} = 8.35^\circ$ for three energies and extrapolated to Q-weak energy $E = 1.155$ GeV in Figure 1.20. Using this hand waving toy model, the obtained BNSSA is $B_n[\text{model}] = 12.15$ ppm at Q-weak kinematics. The asymmetry from this analysis, $B_n[\text{Q-weak}] = 42.27 \pm 15.92$ ppm is also shown in the Figure 1.20. The extrapolation uncertainties are large but cannot be realistically estimated. New calculation are in progress.

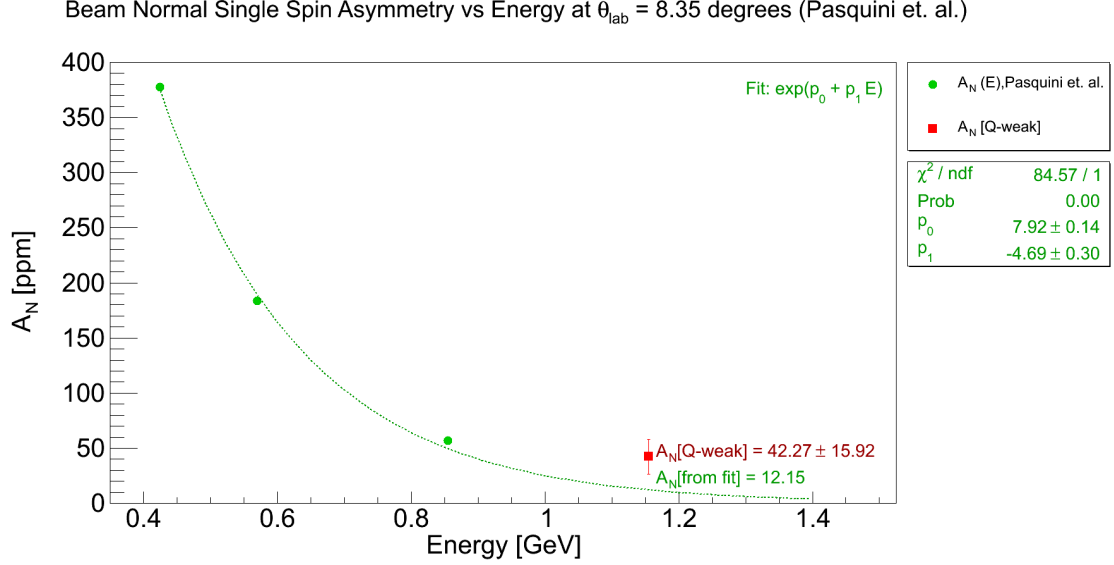


Figure 1.20 BNSSA asymmetry calculation from Pasquini et al. and its extension. The asymmetries from Figure 1.19 at $\theta_{\text{lab}} = 8.35^\circ$ are plotted here. A fit function of the form $f(E) = \exp(p_0 + p_1 E)$ is used to extrapolate the asymmetry to the desired Q-weak kinematic region ($E = 1.155$ GeV).

1.8 BNSSA in Nuclear Targets

In this chapter, the inelastic beam normal single spin asymmetry measurements in e-p scattering have been discussed. In addition to the inelastic data from the proton, Q-weak has data on the beam normal single spin asymmetry measurements from several other physics processes. Few of these measurements are the first of their kind and carry interesting physics. The measured regressed (5+1) asymmetries on liquid hydrogen cell, 4% thick downstream aluminum alloy, and a 1.6% thick downstream carbon foil are summarized in Table ???. The relative statistical precision of the measurements are also shown. The analysis of these data is ongoing and expected to test model calculations of beam normal single spin asymmetry.

1.9 Conclusion

The Q-weak collaboration has made a 35% relative measurement of the beam normal single spin asymmetry of $B_n = 42.27 \pm 2.45$ (stat) ± 15.73 (sys) ppm using transversely polarized 1.155 GeV electrons scattering in-elastically from protons with a Q^2 of 0.0209 (GeV/c)². This is the first measurement of the beam normal single spin asymmetry in inelastic e-p scattering. This measurement

Table 1.9 Measured regressed (5+1) asymmetries in inelastic electron-nucleon scattering for transverse polarized beam. Horizontal and vertical transverse data set are shown separately. The combined (error weighted average) asymmetries are also noted. The inelastic peak is at QTor current 6700 A. The other QTor currents were taken to improve the simulation for elastic radiative tail.

Pol.	Asymmetry [ppm]		
	QTor currents		
	6000 A	6700 A	7300 A
LH ₂			
Hor.	$7.198 \pm 0.688 \pm 0.163$	$5.303 \pm 0.533 \pm 0.092$	$0.717 \pm 0.476 \pm 0.252$
Ver.		$4.457 \pm 0.807 \pm 0.117$	
Both	7.198 ± 0.688 (9.5%)	5.047 ± 0.444 (8.7%)	0.717 ± 0.476 (49.3%)
Al			
Hor.		7.892 ± 1.186	-1.245 ± 1.087
Ver.		9.631 ± 1.768	
Both		8.432 ± 0.985 (11.7%)	-1.245 ± 1.087 (87.3%)
¹² C			
Hor.		10.190 ± 1.863 (18.3%)	

would be an excellent test of theoretical calculations. Unfortunately, at the time of this analysis, there was no existing theoretical calculation or model to compare with the data. Hopefully this thesis will encourage theoreticians to produce new calculations.

REFERENCES

- [1] Q weak Collaboration. The Q-weak Experiment: "A Search for New Physics at the TeV Scale via a Measurement of the Proton's Weak Charge". Technical Report E05-008 Jeopardy proposal, December 2007. (Cited on page 1.)
- [2] P. Pébay. Formulas for robust, One-Pass Parallel Computation of Covariances and Arbitrary-Order Statistical Moments. Sandia Report SAND2008-6212, Sandia National Laboratories, 2008. (Cited on page 3.)
- [3] R. Suleiman, M. Poelker, and J. Grames. Mott Measurements For Hall C. HCLOG-1567146: <https://cebaf.jlab.org/elog/entry/1567146>, February 2011. (Cited on page 5.)
- [4] Shelley Page. Beam: Polarization studies at injector. HCLOG-219054: https://hallcweb.jlab.org/hclog/1102_archive/110208121825.html, February 2011. (Cited on page 5.)
- [5] Buddhini Waidyawansa. *A 3% Measurement of the Beam Normal Single Spin Asymmetry in Forward Angle Elastic Electron-Proton Scattering using the Qweak Setup*. PhD thesis, Ohio University, Athens OH 45701, USA, August 2013. (Cited on pages 6, 23, and 24.)
- [6] Jim Birchall. Effect of averaging over azimuthal angle. ELOG-Analysis-373: <https://qweak.jlab.org/elog/Analysis+Simulation/373>, June 2011. (Cited on page 6.)
- [7] Rakitha Beminiwattha. *A Measurement of the Weak Charge of the Proton through Parity Violating Electron Scattering using the Qweak Apparatus: A 21% Result*. PhD thesis, Ohio University, Athens OH 45701, USA, August 2013. (Cited on page 10.)
- [8] Dave Mack. BCM Normalization Issues Part II: Calibrations and Linearity. Q-weak-DocDB1369: <https://qweak.jlab.org/doc-private/ShowDocument?docid=1369>, March 2011. (Cited on page 13.)
- [9] Dave Mack. Non-linearity Specification for the Qweak Detector Chain. Technical Report Qweak-DocDB-172, November 2004. (Cited on page 13.)
- [10] Joshua Magee. Private communication, 2014. (Cited on page 17.)
- [11] Nuruzzaman. Beam Polarization from Moller Polarimeter for Transverse Run-II Dataset. ELOG-Ancillary-91: <https://qweak.jlab.org/elog/Ancillary/91>, April 2014. (Cited on page 17.)

- [12] Joshua Magee. The Qweak Run 2 Moller Polarimetry Analysis. Technical Report Qweak-DocDB-1955, January 2014. (Cited on page 17.)
- [13] Nuruzzaman. Transverse Asymmetries for N-to-Delta in Nuclear Targets. ELOG-Ancillary-43: <https://qweak.jlab.org/elog/Ancillary/43>, July 2013. (Cited on page 17.)
- [14] Kathrine Myers. *The First Determination of the Proton's Weak Charge Through Parity-Violating Asymmetry Measurements in Elastic e+p and e+Al Scattering*. PhD thesis, The George Washington University, Washington, DC 20052, USA, May 2012. (Cited on page 18.)
- [15] E. D. Cooper and C. J. Horowitz. Vector analyzing power in elastic electron-nucleus scattering. *Phys. Rev. C*, 72:034602, Sep 2005. (Cited on pages 18 and 21.)
- [16] M. Gorchtein and C. J. Horowitz. Analyzing power in elastic scattering of electrons off a spin-0 target. *Phys. Rev. C*, 77:044606, Apr 2008. (Cited on pages 18 and 21.)
- [17] Josh Magee. Aluminum Status Qweak Collaboration Meeting. Hall C collaboration meeting, Q-weak-DocDB1891: <https://qweak.jlab.org/doc-private/ShowDocument?docid=1819>, April 2013. (Cited on page 18.)
- [18] Kent Paschke. Proposed Wien0 neutral beamline background correction. ELOG-Analysis-782: <https://qweak.jlab.org/elog/Analysis++Simulation/782>, October 2012. (Cited on page 20.)
- [19] Manolis Kargiantoulakis. Beamline Backgrounds Update. ELOG-Analysis-1191: <https://qweak.jlab.org/elog/Analysis++Simulation/1191>, July 2014. (Cited on page 20.)
- [20] John Leacock. *Measuring the Weak Charge of the Proton and the Hadronic Parity Violation of the $N \rightarrow \Delta$ Transition*. PhD thesis, Virginia Polytechnic Institute & State University, Blacksburg, VA 24061-0002, USA, October 2012. (Cited on page 20.)
- [21] Dave Mack. Wien0 Beamline Background Dilution Central Value and Uncertainty. ELOG-Analysis-784: <https://qweak.jlab.org/elog/Analysis++Simulation/784>, October 2012. (Cited on page 20.)
- [22] Dave Mack. Input file for Wien 0 elastic e+p asymmetry corrections (v11 frozen modulo unblinding). ELOG-Analysis-714: <https://qweak.jlab.org/elog/Analysis++Simulation/714>, September 2012. (Cited on page 20.)

- [23] Martin McHugh. Neutral Background Analysis. <https://qweak.jlab.org/doc-private/ShowDocument?docid=2072>, September 2014. (Cited on page 20.)
- [24] Rakitha S Beminiwattha. Main Detector Neutral Background Contribution. Technical Report Qweak-DocDB-1549, July 2012. (Cited on page 20.)
- [25] Adesh Subedi. Simulation of QTor scans using QWGEANT3. ELOG-Analysis-837: <https://qweak.jlab.org/elog/Analysis+&+Simulation/837>, December 2012. (Cited on pages 21 and 22.)
- [26] Buddhini Waidyawansa. Qweak Transverse Asymmetry Measurements. Hall C collaboration meeting, Q-weak-DocDB1961: <https://qweak.jlab.org/doc-private/ShowDocument?docid=1961>, February 2014. (Cited on page 21.)
- [27] D. Androic, D. S. Armstrong, A. Asaturyan, T. Averett, J. Balewski, J. Beaufait, R. S. Beminiwattha, J. Benesch, F. Benmokhtar, J. Birchall, R. D. Carlini, G. D. Cates, J. C. Cornejo, S. Covrig, M. M. Dalton, C. A. Davis, W. Deconinck, J. Diefenbach, J. F. Dowd, J. A. Dunne, D. Dutta, W. S. Duvall, M. Elaasar, W. R. Falk, J. M. Finn, T. Forest, D. Gaskell, M. T. W. Gericke, J. Grames, V. M. Gray, K. Grimm, F. Guo, J. R. Hoskins, K. Johnston, D. Jones, M. Jones, R. Jones, M. Kargiantoulakis, P. M. King, E. Korkmaz, S. Kowalski, J. Leacock, J. Leckey, A. R. Lee, J. H. Lee, L. Lee, S. MacEwan, D. Mack, J. A. Magee, R. Mahurin, J. Mammei, J. W. Martin, M. J. McHugh, D. Meekins, J. Mei, R. Michaels, A. Micherdzinska, A. Mkrtchyan, H. Mkrtchyan, N. Morgan, K. E. Myers, A. Narayan, L. Z. Ndukum, V. Nelyubin, Nuruzzaman, W. T. H. van Oers, A. K. Oppen, S. A. Page, J. Pan, K. D. Paschke, S. K. Phillips, M. L. Pitt, M. Poelker, J. F. Rajotte, W. D. Ramsay, J. Roche, B. Sawatzky, T. Seva, M. H. Shabestari, R. Silwal, N. Simicevic, G. R. Smith, P. Solvignon, D. T. Spayde, A. Subedi, R. Subedi, R. Suleiman, V. Tadevosyan, W. A. Tobias, V. Tvaskis, B. Waidyawansa, P. Wang, S. P. Wells, S. A. Wood, S. Yang, R. D. Young, and S. Zhamkochyan. First determination of the weak charge of the proton. *Phys. Rev. Lett.*, 111:141803, Oct 2013. (Cited on page 21.)
- [28] Nuruzzaman. Comparison of H2 Dilutions from Geant-III, IV, and Data at the Inelastic Peak. ELOG-Ancillary-59: <https://qweak.jlab.org/elog/Ancillary/59>, December 2013. (Cited on page 22.)
- [29] Haakon Olsen and L. C. Maximon. Photon and electron polarization in high-energy bremsstrahlung and pair production with screening. *Phys. Rev.*, 114:887–904, May 1959. (Cited on page 23.)

- [30] K. A. Aniol, D. S. Armstrong, M. Baylac, E. Burtin, J. Calarco, G. D. Cates, C. Cavata, J.-P. Chen, E. Chudakov, D. Dale, C. W. de Jager, A. Deur, P. Djawotho, M. B. Epstein, S. Escoffier, L. Ewell, N. Falletto, J. M. Finn, K. Fissum, A. Fleck, B. Frois, J. Gao, F. Garibaldi, A. Gasparian, G. M. Gerstner, R. Gilman, A. Glamazdin, J. Gomez, V. Gorbenko, O. Hansen, F. Hersman, R. Holmes, M. Holtrop, B. Humensky, S. Incerti, J. Jardillier, M. K. Jones, J. Jorda, C. Jutier, W. Kahl, D. H. Kim, M. S. Kim, K. Kramer, K. S. Kumar, M. Kuss, J. LeRose, M. Leuschner, D. Lhuillier, N. Liyanage, R. Lourie, R. Madey, D. J. Margaziotis, F. Marie, J. Martino, P. Mastromarino, K. McCormick, J. McIntyre, Z.-E. Meziani, R. Michaels, G. W. Miller, D. Neyret, C. Perdrisat, G. G. Petratos, R. Pomatsalyuk, J. S. Price, D. Prout, V. Punjabi, T. Pussieux, G. Quémener, G. Rutledge, P. M. Rutt, A. Saha, P. A. Souder, M. Spradlin, R. Suleiman, J. Thompson, L. Todor, P. E. Ulmer, B. Vlahovic, K. Wijesooriya, R. Wilson, and B. Wojtsekhowski. Measurement of the neutral weak form factors of the proton. *Phys. Rev. Lett.*, 82:1096–1100, Feb 1999. (Cited on page 23.)
- [31] K. A. Aniol, D. S. Armstrong, T. Averett, M. Baylac, E. Burtin, J. Calarco, G. D. Cates, C. Cavata, Z. Chai, C. C. Chang, J.-P. Chen, E. Chudakov, E. Cisbani, M. Coman, D. Dale, A. Deur, P. Djawotho, M. B. Epstein, S. Escoffier, L. Ewell, N. Falletto, J. M. Finn, K. Fissum, A. Fleck, B. Frois, S. Frullani, J. Gao, F. Garibaldi, A. Gasparian, G. M. Gerstner, R. Gilman, A. Glamazdin, J. Gomez, V. Gorbenko, O. Hansen, F. Hersman, D. W. Higinbotham, R. Holmes, M. Holtrop, T. B. Humensky, S. Incerti, M. Iodice, C. W. de Jager, J. Jardillier, X. Jiang, M. K. Jones, J. Jorda, C. Jutier, W. Kahl, J. J. Kelly, D. H. Kim, M.-J. Kim, M. S. Kim, I. Kominis, E. Kooijman, K. Kramer, K. S. Kumar, M. Kuss, J. LeRose, R. De Leo, M. Leuschner, D. Lhuillier, M. Liang, N. Liyanage, R. Lourie, R. Madey, S. Malov, D. J. Margaziotis, F. Marie, P. Markowitz, J. Martino, P. Mastromarino, K. McCormick, J. McIntyre, Z.-E. Meziani, R. Michaels, B. Milbrath, G. W. Miller, J. Mitchell, L. Morand, D. Neyret, C. Pedrisat, G. G. Petratos, R. Pomatsalyuk, J. S. Price, D. Prout, V. Punjabi, T. Pussieux, G. Quémener, R. D. Ransome, D. Relyea, Y. Roblin, J. Roche, G. A. Rutledge, P. M. Rutt, M. Rvachev, F. Sabatie, A. Saha, P. A. Souder, M. Spradlin, S. Strauch, R. Suleiman, J. Templon, T. Teresawa, J. Thompson, R. Tieulent, L. Todor, B. T. Tonguc, P. E. Ulmer, G. M. Urciuoli, B. Vlahovic, K. Wijesooriya, R. Wilson, B. Wojtsekhowski, R. Woo, W. Xu, I. Younus, and C. Zhang. Parity-violating electroweak asymmetry in $\bar{e}p$ scattering. *Phys. Rev. C*, 69:065501, Jun 2004. (Cited on page 23.)
- [32] Peiqing Wang. Simulated octant-by-octant event rate, scattering angle and momentum trans-

- fer. ELOG-Analysis-589: <https://qweak.jlab.org/elog/Analysis+&+Simulation/589>, May 2012. (Cited on page 24.)
- [33] Nuruzzaman. Q^2 for transverse N-to-Delta from GEANT-III. ELOG-Ancillary-44: <https://qweak.jlab.org/elog/Ancillary/44>, July 2013. (Cited on page 24.)
- [34] Andrei V. Afanasev and N.P. Merenkov. Collinear photon exchange in the beam normal polarization asymmetry of elastic electron-proton scattering. *Physics Letters B*, 599(1?2):48 – 54, 2004. (Cited on page 25.)
- [35] Barbara Pasquini. Two-Photon Physics: Theory. MAMI and Beyond: <http://wwwkph.kph.uni-mainz.de/T//MAMIandBeyond/02%20Dienstag/08%20Pasquini.pdf>, April 2009. (Cited on page 27.)
- [36] Constantia Alexandrou, Tomasz Korzec, Giannis Koutsou, Cdric Lorc, John W. Negele, Vladimir Pascalutsa, Antonios Tsapalis, and Marc Vanderhaeghen. Quark transverse charge densities in the from lattice {QCD}. *Nuclear Physics A*, 825(1-2):115 – 144, 2009. (Cited on page 27.)